

www.acsami.org Research Article

RNA Sequencing at Single Vesicle Resolution via 3D Printed Embedded Droplet Arrays

Andrew A. Brock,[‡] Senthilkumar Duraivel,[‡] Jinmai Jiang, Jonathan Fischer, Zachary F. Greenberg, Mei He, Thomas E. Angelini,* and Thomas D. Schmittgen*

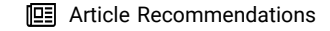


Cite This: https://doi.org/10.1021/acsami.5c09959

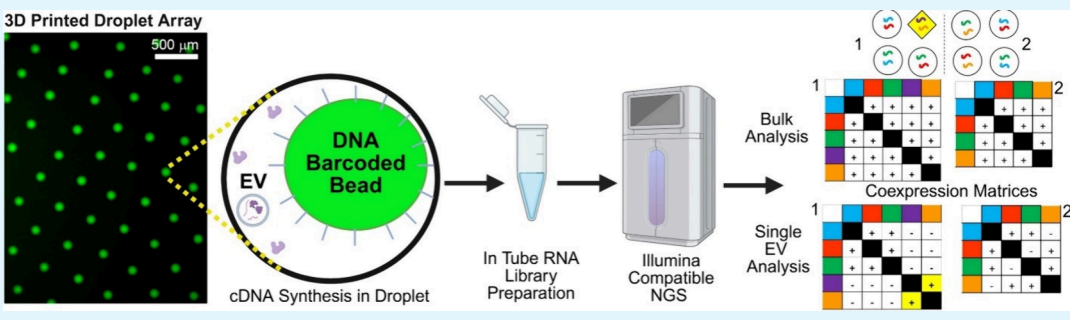


ACCESS

Metrics & More



sı Supporting Information



ABSTRACT: Single-cell RNA sequencing has transformed our understanding of cellular heterogeneity; however, comparable methods for studying individual extracellular vesicles (EVs) remain scarce. To address the heterogeneity of RNA cargo contained within EVs, we developed a platform that 3D prints droplet arrays that generate cDNA for sequencing single EVs. The printing method leverages the interfacial instability between a hydrocarbon-based support material and printed aqueous solutions, driving printed features to break up into controllable, homogeneous droplets of a desired size that become stably trapped in 3D space. We printed picoliter aqueous droplets of EVs, DNA barcoded oligonucleotide beads, and biochemicals and performed a variety of reactions within the organogel support medium including PCR and synthesis of poly(A)⁺ RNA sequencing compatible cDNA. Printing conditions were optimized to ensure ideal droplet loading of individual barcoded beads and single EVs within each droplet. Following collection of aqueous cDNA material from the organogel, additional biochemical reactions were performed in tubes in order to generate sequencable RNA libraries. Individual CD9, CD63, and CD81 positive EVs contained a wide variety of poly(A)⁺ RNAs including mRNA, mitochondrial RNA, and noncoding RNAs. Poly(A)⁺ RNAs of individual 100 nm immunopurified THP-1 EVs were sequenced using the 3D printing method and identified 3689 unique barcodes with at least two corresponding reads of poly(A)⁺ RNA per EV, and the average amount of poly(A)⁺ RNA per EV was 3.32. The developed platform resolves EV poly(A)⁺ RNA heterogeneity with potential implications for biomarker discovery and other clinical applications.

KEYWORDS: extracellular vesicles, exosomes, 3D printing, RNA sequencing, cellular heterogeneity, droplet manufacturing

INTRODUCTION

Extracellular vesicles (EVs) are nanosized lipid bilayer vesicles produced by cells that contain nucleic acids, proteins, metabolites and lipids. Released by nearly all cell types, EVs play critical roles in many pathological and physiological processes including cancer metastases, coagulation, inflammatory response, cell maturation, adaptive immune response, bone calcification and neural cell communication. EVs contain a variety of nucleic acid cargo including mRNA, miRNA, long and short noncoding RNAs, tRNA, rRNA, and their fragments. There is broad clinical potential for EVs as therapeutics and diagnostics due to their stability in the bloodstream and ability to functionally transfer their cargo to recipient cells. An impediment to furthering our understanding of the role EVs play in biology, physiology and disease is the vast heterogeneity in vesicle structure, composition,

content and function.⁵ EV heterogeneity is often masked as most studies of their functional significance investigate EVs in bulk and use ensemble-averaging assays (i.e., 'omics') for data interpretation.⁶ One way to assess the functional heterogeneity of EVs is to study their properties on an individual level.

Current methods to perform single EV detection (e.g., TEM, dynamic light scattering, atomic force microscopy, etc.) may visualize the EV but fail to gather molecular or high throughput analyses. Principle Component Analysis of Raman spectro-

Received: May 20, 2025 Revised: September 1, 2025 Accepted: September 2, 2025



Research Article

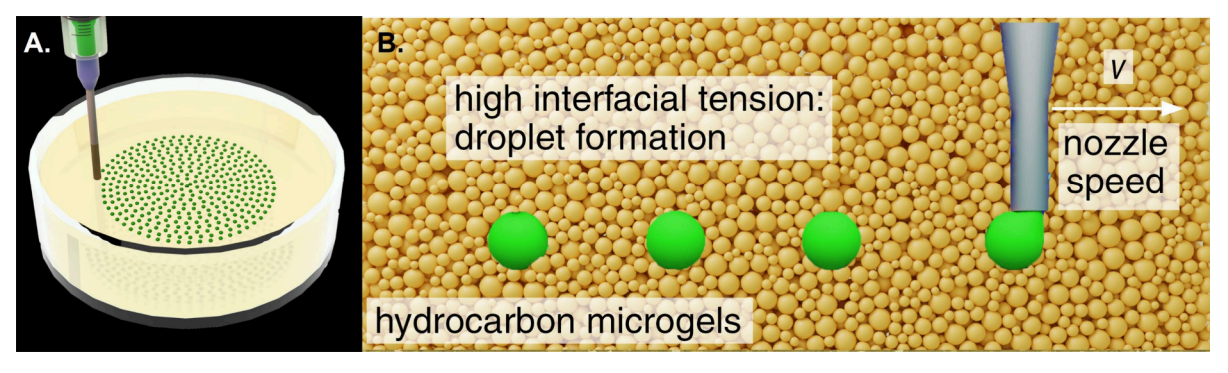


Figure 1. Schematic overview of 3D printing droplet manufacturing. Embedded 3D printing of aqueous inks in high interfacial support materials like organic microgels leads to the break of the printed features into droplets. (A) An array of 3D printed droplets trapped in a support medium made from packed micro-organogels. (B) By leveraging the interfacial instability driven breakup of the deposited ink, embedded printing of picodroplets is achieved, with high homogeneity and high droplet production rates.

scopic data examined the chemical composition of individual EVs isolated from cancer cell lines and showed sources of spectral variation among the EVs in terms of their cholesterol content and surface protein expression. Raman spectroscopy combined with multispectral optical tweezers allowed for the molecular fingerprinting of subpopulations of mesenchymal stem cell EVs. Zhang et al., applied asymmetric flow field-flow fractionation (AF4) and identified two EV subpopulations with distinct biophysical and molecular (proteomic, lipidomic and glycomic) properties. Additional single vesicle analysis methods have been achieved to evaluate surface proteins of individual EVs by combining microfluidics and antibody-based immunosequencing methods 10,11 as well as immunocapture and imaging analysis of EVs for determining specific protein and RNA species. 11,12 The polyadenylated RNA contents of individual large EVs isolated from a low-speed centrifugation fraction (16,000 \times g) were sequenced using 10x Genomics Chromium single cell sequencing platform. 12 Using this platform, insights on EV RNA cargo heterogeneity were gained, however, the analysis was limited to include only large EVs (approximately mean diameter 250 nm). Thus, while several innovative approaches have been developed to examine the properties of individual EVs, none to our knowledge are able to perform RNA sequencing of individual small EVs (\sim 100 nm diameter).

High-throughput sequencing of individual EVs within large and heterogeneous populations is analogous to single cell RNA sequencing. An early challenge in developing single-cell genome sequencing technologies was the difficulty of encapsulating single cells within individual drops which could be used as PCR vessels.¹³ Advanced microfluidic technologies have been developed for triggering the formation of droplets at the instant that a single cell enters a fluidic orifice, creating "drops on demand" containing single cells. 14 At the nanoscale, microfluidic technology has been hampered by low throughput and susceptibility to clogging of the nanofluidics. 15 Moreover, the microfluidics systems are unable to reliably detect 100 nm EVs. The disadvantage of both approaches to encapsulating single cells is that sophisticated microfluidic devices must be specifically designed and closely controlled by technical experts, limiting their utility outside of specialized academic laboratories and core research facilities. 16

We report on the development of an integrated platform that combines embedded 3D printing methods and materials with molecular barcoding technology for performing biochemical reactions within individual droplets that enables the

RNA sequencing of individual EVs. To avoid the technical challenges associated with microfluidic cell encapsulation, we leveraged a recently developed 3D printing method designed specifically for creating shapes from fluid phases and trapping them stably in 3D space. ^{17–20} This approach has been effective at creating stable structures made from aqueous polymers, colloidal particles, living cells, silicone elastomers, and liquid oil. 18,21 Using our platform, we 3D printed biochemical reactions and produced approximately 20,000 droplets in the microgel, with approximately 3,500 of these droplets containing one barcoded bead and one EV for individual EV RNA sequencing. A series of biochemical reactions were performed in the organogel to demonstrate the feasibility of generating sequenceable cDNA. Test runs were completed on ultracentrifugation isolated and immunoaffinity purified isolation of EVs. Greater than 3500 individual EVs were sequenced in this 3D printing platform, providing the very first example of the poly(A)⁺ cargo of individual EVs in the 100 nm size range.

■ RESULTS AND DISCUSSION

To generate liquid droplets that encapsulate individual EVs along with single barcoded beads and sequencing reagents, we leverage an oily hydrocarbon-based support material that was originally developed for 3D printing silicone structures. The support material is made from a mixture of block copolymers and mineral oil with no added surfactants or rheological modifiers²⁰ (see Materials and Methods for formulation details). The block copolymers self-assemble into stable, micron-scale, gel particles that swell in mineral oil, known as micro-organogels. The micro-organogels are $2-4 \mu m$ in diameter under dilute conditions. When sufficiently packed, the micro-organogels form a jammed macroscopic solid that yields and rearranges in response to a translating printing nozzle while maintaining a solid-like character under shear stresses less than its yield stress of 3-4 Pa. For 3D printing applications, this yielding behavior sets a minimum stable feature diameter given by $d_m = \gamma/\sigma_v$, where γ is the interfacial tension between the printed feature and the support material, and σ_{v} is the yield stress of the support material. For droplet generation, by contrast, we intentionally make use of the high interfacial tension between extruded aqueous solutions and the oily surroundings of approximately 40 mN/m, operating in a regime where extruded filaments are not stable. However, much like the 3D printing technique, once droplets are formed, they are trapped in space for processing, collection, and

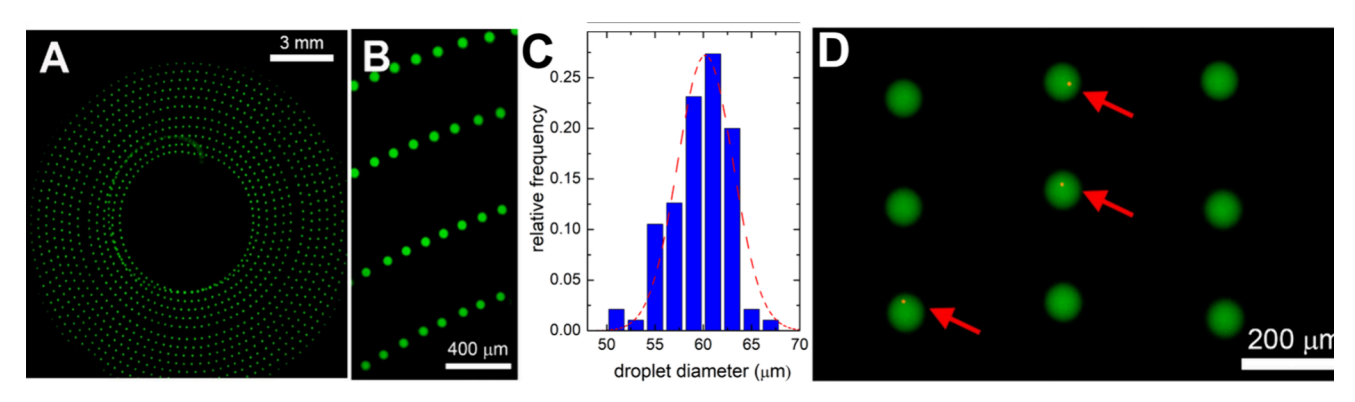


Figure 2. 3D printing as a platform for biochemical reactions. (A) To 3D print homogeneous arrays of droplets, we generated a spiral pattern of approximately 1100 rhodamine droplets and imaged them using epifluorescence microscopy (green pseudocolor to enhance visualization). The droplets are trapped in space, held in place by an organic microgel support medium. (B) Enlarged image of part A. (C) The relative frequency of the droplet diameters follows a Gaussian distribution (red dotted line), with a mean diameter (\pm standard deviation) of 60.2 \pm 2.8 μ m. (D) To test our ability to control the distribution of EVs within 3D printed droplets, experiments were performed using 100 nm fluorospheres in place of EVs; droplets filled with rhodamine solution (green) can be seen to contain single fluorospheres (arrows).

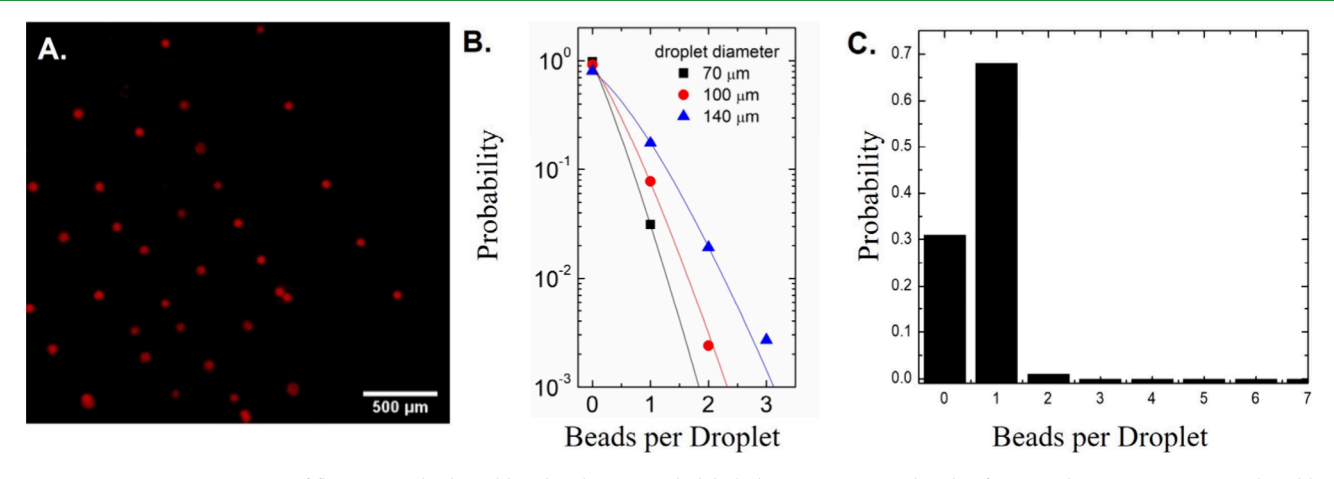


Figure 3. Printing optimization of fluorescent hydrogel beads. Fluorescently labeled BDP-conjugate beads of 63 μ m diameter were printed at dilute concentrations to generate droplets having diameters of 70, 100, and 140 μ m. (A) Representative image of BDP-conjugated hydrogel beads following 3D printing to generate 70 μ m droplets. Scale bar is 500 μ m. (B) The probability distributions of loading different numbers of beads per printed droplet were determined using confocal microscopy and were found to fit to the Poisson distribution (lines). (C) Switching from dilute suspensions to printing with close-packed beads increased the probability of printing exactly one of the 63 μ m diameter fluorescently labeled beads per droplet to approximately 67% while the remaining droplets were empty. More than one bead per drop occurred less than 2% of the time a droplet was generated.

analysis (Figure 1). We tested this approach by translating a printing nozzle through the support material while extruding an aqueous rhodamine solution, generating more than 1000 droplets in a few seconds, finding that the droplets remain stably trapped in space (Figure 2A,B).

To test our ability to control the distribution of EVs in printed droplets and to detect individual EVs within droplets following the 3D printing procedure, we performed tests using 100 nm diameter fluorospheres as surrogate EVs, dispersed in aqueous rhodamine solutions. We chose the fluorosphere concentration based on the Poisson distribution, ¹³ aiming for a concentration where most droplets were empty, approximately 5% contained one fluorosphere, and a negligible number contained more than one sphere (see Supporting Information for Publication file). Translating the printing nozzle at $\nu=20$ mm/s and depositing the nanoparticle suspension at a rate of $Q=150~\mu\text{L/h}$, we produced a spiraling array of droplets roughly 60 μ m in diameter spaced approximately by 100 μ m (Figure 2C). Epifluorescence images of the droplet arrays after

printing showed that most droplets were either empty or contained one fluorosphere (Figure 2D).

The statistics of low concentrations are often leveraged in encapsulation approaches where the number of objects per capsule is sure to be stochastic, as occurs with diffusing particles or randomly dispersed cells in microfluidic devices. 22-24 To test our ability to leverage such statistics, we dispersed 63 µm diameter "dummy beads" that lack oligonucleotide barcoding into dPBS buffer. Using this dispersion, we printed droplet arrays before the beads were able to settle out of solution. Counting the number of beads encapsulated per droplet, we found the encapsulation probability was well described by the Poisson distribution, where most droplets were empty, and the probability of encapsulating a specific number of beads decreased exponentially with the number encapsulated. We also found that the distribution was sharper for smaller droplet diameters, which is expected in this limit because the droplets became too small to accommodate larger numbers of beads (Figure 3B).

Using dilute dispersions of 63 μ m diameter beads and generating 70 μ m diameter droplets resulted in approximately 97% empty droplets and 3% containing one bead. This is close to the optimal efficiency sought in microfluidic encapsulation, where 95% of droplets are empty and roughly 5% contain one object. To improve on this result, we developed an approach in which the beads are close-packed and the inner diameter of the printing nozzle is slightly larger than the diameter of the beads. With this strategy, we aimed to force the beads into a single-file line without any large gaps between them (Figure 4). Using a

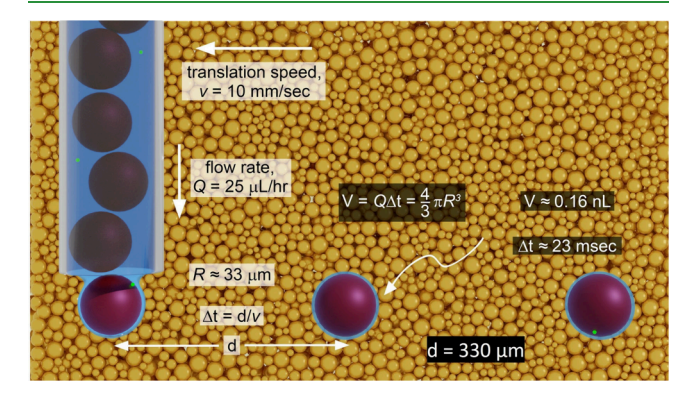


Figure 4. Strategy for loading closely packed barcoded beads. To maximize the sequencing of encapsulated single EVs within printed droplets, translation speed and flow rate were optimized to achieve a \sim 70 μ m diameter aqueous droplet through a 120 μ m diameter needle. The \sim 100 nm EV (green dot, not to scale) and 63 μ m barcoded DNA hydrogel bead (purple ball) will be embedded within the droplets spaced at about 330 μ m from each other. Droplets are printed at a rate of approximately 1 per 23 ms.

26s gauge RN stainless-steel needle, which has an inner diameter of 120 μ m, we adjusted the translation speed and volumetric deposition rate until we achieved the highest proportion of droplets contained one barcoded bead. In this case, $v=10~\mu\text{m/s}$ and $Q=25~\mu\text{L/h}$, which ideally is expected to result in a droplet spacing of approximately 150 μ m. Analyzing epifluorescence images of the droplet arrays, we found the average spacing to be 330 μ m, within approximately a factor of 2 of the ideal case (Figure 3A). More importantly, counting the number of encapsulated beads per droplet, we

found that 31% of droplets were empty while 67% of printed droplets contained one bead. The remaining 2% contained two beads (Figure 3C).

The high efficiency of bead encapsulation indicates that even if the efficiency of EV encapsulation is low, the combined probability of encapsulating a single barcoded bead and a single EV will be relatively high. Guided by our preliminary tests using 100 nm fluorospheres, we switched to fluorescently labeled EVs and further refined our printing parameters. HEK293T EVs were stained with a cell-permeant fluorescent dye to selectively stain RNA within EVs. The packed BDPconjugated beads and EVs (350 EVs/ μ L) were printed using a translation speed $\nu = 20$ mm/sec at a flow rate of $Q = 3 \mu L/h$ (Figure 5A). Confocal fluorescence microscopy was used to observe stained EVs along with BDP-conjugated beads that were contained within each droplet (Figure 5B). Images of individual droplets were analyzed to determine the number of EVs that contain 0, 1, 2 or more in each droplet containing a bead. We found that 25% of bead-containing droplets contained one EV, 73% contained no EVs and the remaining 2% contained 2 EVs (Figure 5C). Combining the 67% efficiency of encapsulating one barcoded bead with the 25% probability that each of these droplets will contain one EV, the overall efficiency of this encapsulation strategy is approximately

Conditions To Synthesize cDNA within 3D Printed Droplets. Before generating sequencable cDNA within printed droplets, it was necessary to demonstrate that the aqueous biochemical reactions within the support medium can be moved into reaction tubes post printing. To demonstrate the transfer of aqueous droplets from the hydrocarbon-based gel, an aqueous solution of bromophenol blue was delivered into the microgel material and then briefly centrifuged (Figure 6A). To demonstrate our ability to perform biochemical reactions within the embedded droplets, RT-PCR was performed on the printed droplets containing a 1-step RT-PCR cocktail, DNase treated mouse liver RNA and primers to the 18S rRNA gene. The amplified 18S rRNA product from the in-gel reaction was detectable (Figure 6B).

Next, a series of reactions with total HEK293T EV RNA or synthetic poly(A) $^+$ luciferase mRNA was 3D printed (Figure 6C). To prime the RNA for cDNA synthesis, oligo(dT) was

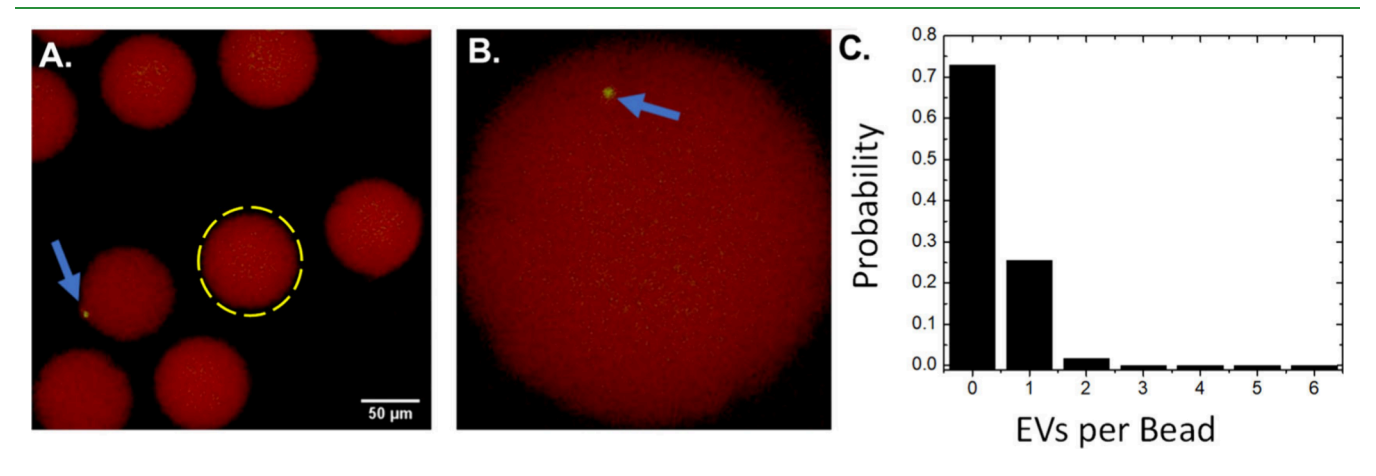
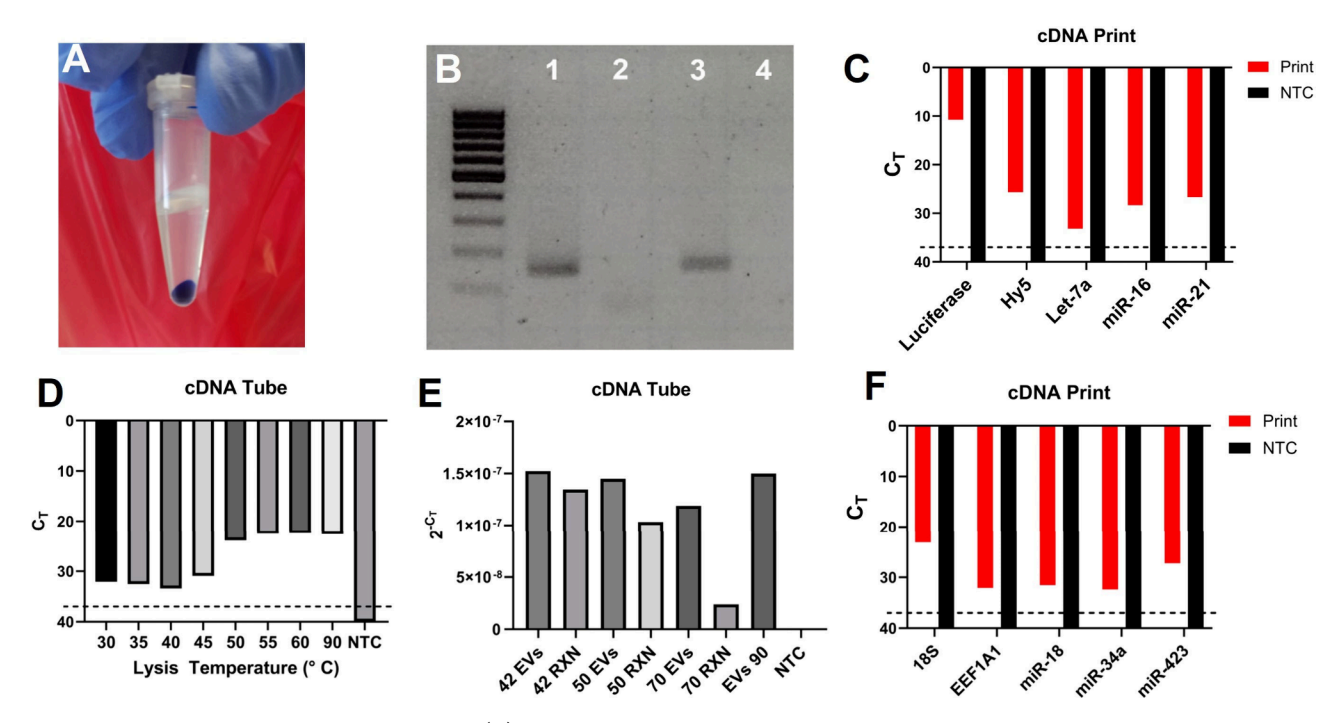


Figure 5. EV printing conditions to optimize single droplet loading. (A) Confocal images of a single green-labeled EVs (arrows) within a droplet containing one red BDP-conjugated bead (yellow dashed line). Scale bar is 50 μ m. (B) Zoomed-in image of BDP-conjugated bead and SYTO RNASelect Green EV. (C) The probability of printing zero, one, or \geq 2 EVs per droplet as determined from confocal images of droplets. The probability of printing 1 EV per droplet when at a concentration of 350 EVs/ μ L is 25%. Images collected with 60× objective.



www.acsami.org

Figure 6. Biochemical reactions in micro organogel. (A) An aqueous solution of bromophenol blue was pipetted into a sample of microgel material and then centrifuged. The separated aqueous material can be seen clearly at the bottom of the microcentrifuge tube. (B) To test whether biochemical reactions can be performed in microgel, RT-PCR was performed within a 3D printed droplet array. Droplets were generated with a reaction of isolated mouse liver total RNA and reagents for a one-step RT-PCR. After thermocycling, the aqueous and gel components were separated as in (A) and the amplified cDNA product was resolved by 1.5% agarose gel electrophoresis. Lane 1, Amplicon of 18S rRNA printed; 2, minus RT control in printed gel; 3, cDNA positive control in tube; and 4, NTC PCR. GeneRuler 100 bp DNA Ladder was used. (C) RT reactions were performed with isolated/purified RNA samples of HEK293T EV RNA (150 ng) or luciferase mRNA (250 ng) primed with stem-loop primers and oligo(dT), respectively. Following aqueous phase separation, gene expression analysis of isolated cDNA was subjected to qPCR analysis and data are presented as mean C_T values in triplicate. (D) \sim 10⁷ HEK293T EVs in RT buffer were exposed to lysis temperatures for 5 min and then cooled on ice. Then the remaining RT reagents were added including the RT enzyme, followed by reverse transcription at 50 °C for 2 h. qPCR analysis was performed on miR-10b-5p, and data are presented as mean C_T values in triplicate. (E) Additional lysis and thermal stability experiments were performed in tube to expose HEK293T EVs and whole reverse transcription reactions to different temperatures. Gene expression analysis of isolated cDNA was subjected to qPCR analysis of U6, and data are presented as mean 2^{-C_T} values in triplicate. (F) HEK293T EVs were printed in bulk and reverse transcription was performed with random hexamers and stem loop adaptors. Gene expression analysis of isolated cDNA was subjected to qPCR analysis and data are presented as mean C_T value

used for luciferase mRNA, and stem-loop RT primers were used to prime the mature miRNA contained within HEK293T EVs. Following printing, the gel medium was heated to 50 °C for 2 h to perform the reverse transcription reaction using a thermostable reverse transcriptase. Following separation of the organic and aqueous phases, in-tube PCR of the cDNA indicated successful amplification of multiple expressed genes above the level of detection (Figure 6C).

Prior to performing biochemical reactions with EVs, they were characterized based on the International Society of Extracellular Vesicles (ISEV) standards.²⁶ EVs of a median of 108 nm were isolated. EVs displayed a clearly defined bilayer membrane and expression of proteins common to EVs (CD63) by Western blotting (Figure S2). Biochemical reactions with purified EVs were performed to demonstrate efficient EV lysis and the ability to capture RNA for cDNA synthesis (Figure 6D). Additional experiments were performed to determine the optimal temperature for efficient lysis and reverse transcriptase activity (Figure 6E). The reverse transcription in-tube control was primed with stem-loop adaptor for miR-10b-5p (Figure 6D) or stem-loop adaptor for U6 RNA (Figure 6E). The efficiency of the 50 °C reaction was comparable to the 90 °C lysed EVs with cooling control. Next, HEK293T EVs were printed, and a reverse transcription

reaction was performed at 50 $^{\circ}$ C for 2 h to lyse EVs and generate cDNA. Multiple expressed genes were detected by PCR demonstrating efficient EV lysis and reverse transcription (Figure 6F).

Next, we designed a reverse transcription primer mimicking the photocleavable oligos on the barcoded DNA hydrogel beads to perform 3D printed microgel reactions. This primer was similar to that of the barcoded DNA oligo RT primer, except it does not contain the T7 transcription start site and PE1 adaptor site (Figure S1B). As a positive control, we performed qRT-PCR in tubes with HEK293T cellular RNA and EV RNA (Figure S4A). 18S rRNA, EEF1A1, and FTL were all detectable above the limit of detection following qPCR analysis. Next, we performed identical reactions following 3D printing in the organogel (Figure S4B). Following isolation of the aqueous phase, qPCR was used to analyze the cDNA product of the 3D printed reaction. Mouse liver synthesized cDNA was positive for B-Actin and EV cDNA expressed Eef1a1 and Ftl above the limit of detection. All NTCs were C_T s of 40 (i.e., undetectable).

cDNA was synthesized with the barcoded DNA hydrogel beads following 3D printing. A mixture of EVs or RNA, barcoded hydrogel beads and biochemicals were 3D printed and the reverse transcription reaction was performed in the

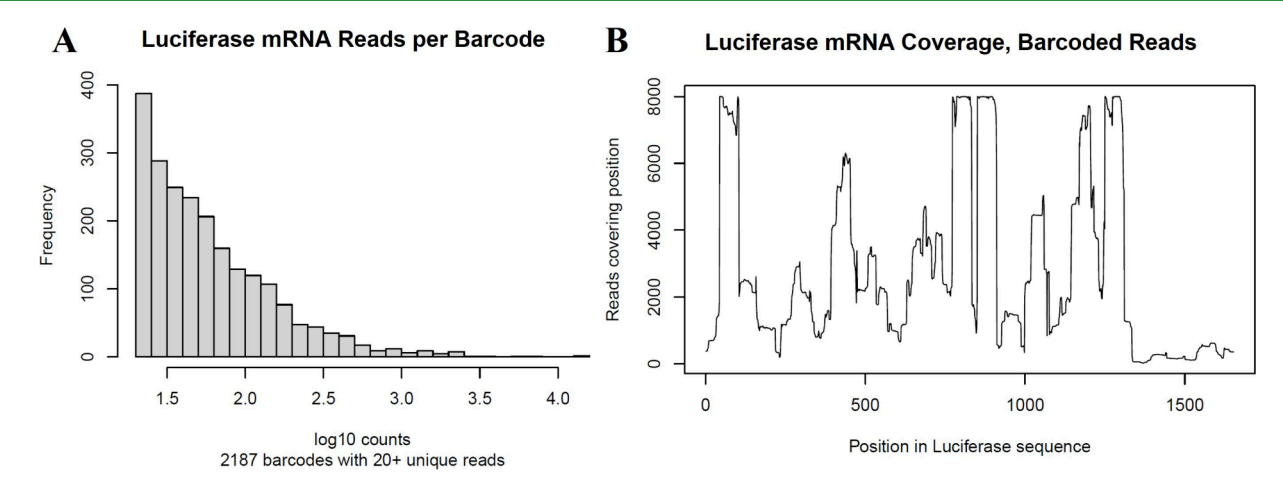


Figure 7. RNA reads per barcode and coverage for sequencing luciferase mRNA. (A) For a sample of luciferase mRNA (50 ng), the distribution of unique reads per barcode is displayed after restricting barcodes with at least 20 reads. (B) Captured reads were aggregated across barcodes to examine coverage of the luciferase transcript. The coverage value corresponds to the number of reads spanning the given position after read

support medium. Bulk EV or EV RNA prints using the barcoded DNA hydrogel beads were performed with approximately 10⁷ EVs or 50 ng, respectively. Following cDNA synthesis, enzymatic cleanup of unused barcodes and an overnight in vitro transcription reaction, a second reverse transcription was performed in-tube. qPCR analysis indicated the presence of the PCR products above the level of detection (Figure S4C,D).

HEK293T EVs were printed in bulk and at single EV conditions and following a similar postprinting workflow outlined in Figure S4C qPCR detected the expression of EEF1A1 and FTL comparing bulk and single EV prints within 1 C_T of each other (Figure S3D). These results demonstrate our ability to synthesize cDNA within droplets suspended in the microgel using the stem loop RT primers to mature miRNAs, oligo(dT), and DNA oligos mimicking those found on the barcoded DNA hydrogel beads.

Optimized 3D Printing for RNA Sequencing. To demonstrate the synthesis of sequenceable cDNA in printed droplets, we printed and processed sequencing libraries from 50 ng of synthetic poly(A)+ luciferase mRNA. Subsequent NovaSeq 6000 sequencing generated 3.3×10^8 raw reads. The distribution of unique reads per barcode for those exceeds the threshold of 20 reads per barcode (Figure 7A) indicating that >2,000 barcodes, and over 200,000 unique luciferase reads were captured in total. A median of 47 reads is captured per barcode of which 90% of captured reads correspond to luciferase. A luciferase mRNA coverage plot (Figure 7B) shows where the captured reads aggregated to examine coverage of the entire luciferase mRNA transcript. Notably, the limited coverage in the 3' region of luciferase mRNA occurs just before the proprietary 3' UTR sequence of Trilink's luciferase mRNA. These data demonstrate our ability to perform biochemical reactions in picoliter droplets, recover the printed material, and generate RNA sequencing libraries following our 3D printing platform.

Single EV Sequencing via 3D Printing. Next, we sought to culminate the approach to 3D print and perform RNA sequencing of individual EVs. The overall schema to perform single EV RNA sequencing is depicted in Figure S1A. Highly pure, ~100 nm CD9⁺, CD63⁺ and CD81⁺ EVs were isolated from THP-1 cells were used in the printing. Optimized

printing conditions were used in which the number of droplets containing one barcoded bead and one EV is maximized, while the droplets containing multiple EV and/or barcoded beads are negligible. An aqueous suspension of THP-1 immunopurified EVs, barcoded hydrogel beads and reverse transcription biochemicals were 3D printed. Approximately 20 thousand droplets were printed in ~30 min producing an estimated 3,500 droplets that contained one EV and one barcoded gel bead. Following subsequent workup including a final in vitro transcription step, the resulting RNA revealed the presence of intact poly(A)+ RNA of 200 to 6,000 nts in length (average 3,537 nt) (Figure S3A). Following a second reverse transcription primed with either oligo dT for the poly(A)⁺ RNA or stem-loop primers for mature miRNA, the cDNA was assayed by qPCR. The C_T s of the poly $(A)^+$ RNA were above the assay's limit of detection while mature miRNA was undetectable (Figure S3C). After RNA sequencing and bioinformatic analysis, 3689 individual barcodes were identified following data processing and read alignment to the genome. The 10 most abundantly expressed genes include several protein coding, mitochondrial and long noncoding RNAs (Table 1). Several of the top expressed genes identified have been reported as abundantly expressed in author Luo et al., EVs (MALAT1, ND4)¹² or Wang et al., EVs (RNR2).²⁷

Table 1. Top 10 Expressed Genes Identified in CD9⁺, CD63⁺, CD81⁺ THP-1 Single EVs

| Gene | Number of Barcoded Reads | Gene Class | Mitochondrial Gene |
|-----------|--------------------------------|---------------------|-----------------------|
| MT-RNR2 | 831 | 16S rRNA | Yes |
| MTRNR2L12 | 563 | 16S rRNA Pseudogene | Yes |
| MT-CYB | 314 | Protein Coding | Yes |
| ARHGEF40 | 143 | Protein Coding | No |
| MT-ND4 | 139 | Protein Coding | Yes |
| CUBN | 99 | Protein Coding | No |
| DANCR | 97 | lncRNA | No |
| FBXW7 | 92 | Protein Coding | No |
| MTRNR2L1 | 86 | 16S rRNA Pseudogene | Yes |
| PROZ | 83 | Protein Coding | No |
| | | | |

Additionally, we 3D printed and sequenced ~ 3500 individual HEK293T EVs that were isolated by ultracentrifugation. Following RNA sequencing and bioinformatic analysis using the sequencing pipeline, 1099 individual barcodes were identified and aligned to the genome. The resulting RNA revealed the presence of intact poly(A)⁺ RNA of 200 to 6,000 nts in length (Figure S3B). The 10 most abundantly expressed genes were ranked (Table 2) and include

Table 2. Top 10 Genes Identified in UC Purified HEK293T Single EVs

| Gene | Number of Barcoded Reads | Gene Class | Mitochondrial Gene |
|---------------|--------------------------------|---------------------|-----------------------|
| ARHGEF40 | 222 | Protein Coding | No |
| EVI5L | 157 | Protein Coding | No |
| MT-RNR2 | 109 | 16S rRNA | Yes |
| FBXW7 | 93 | Protein Coding | No |
| MTRNR2L12 | 90 | 16S rRNA Pseudogene | Yes |
| MT-CYB | 22 | Protein Coding | Yes |
| DANCR | 20 | lncRNA | No |
| PROZ | 19 | Protein Coding | No |
| RP11-507B12.2 | 14 | LincRNA | No |
| ST18 | 12 | Protein Coding | No |

several protein coding, mitochondrial and long noncoding RNAs. A comparison revealed much less unique cell barcodes in the ultracentrifugation purified compared to the immunoaffinity purified EVs even though the same number of EVs were printed for each sample.

Interestingly 6 of the top 10 expressed genes identified from EVs of different cellular origin, purified by two different methods overlapped (Tables 1 and 2). Of these 6 overlapping genes, 4 are either mitochondrial RNAs or are involved in regulating mitochondrial function (i.e., FBXW7). Table 3

Table 3. Single EV RNA Sequencing Statistics

| | THP-1 EVs | HEK293T EVs |
|--|-----------|-------------|
| Estimated Number of Printed Single EVs | 3500 | 3500 |
| Number of Barcodes (EVs) | 3689 | 1099 |
| Average Number of Reads | 3.32 | 2.14 |
| Average Number of Genes | 2.35 | 2.01 |
| Mode of Reads per EV | 2 | 2 |
| Mode of Genes per EV | 2 | 2 |
| Range of Reads per EV | 2-33 | 2 - 11 |
| Range of Genes per EV | 1-12 | 1-5 |

illustrates similarities and differences in the number of reads and expressed genes per EV in the THP-1 and HEK293T EVs. The range of reads per EV spanned from 2–33 and 2–11 in THP-1 immunopurified EVs and HEK393T UC purified EVs, respectively. The range of expressed genes per EV varied from 1 – 12 and 1 – 5 in THP-1 immunopurified EVs and HEK393T UC purified EVs, respectively. The number of unique barcodes (i.e., single EV) identified from the RNA sequencing corresponds to the number individual EVs that were printed (~3500) for that sample (Table 3, Table S1, Table S2). The average number of poly(A)⁺ RNA reads per EV was 3.32 and 2.14 for THP-1 and HEK293T EVs, respectively. The average number of expressed genes per EV was similar at 2.35 and 2.01 for THP-1 and HEK293T, respectively. The sequencing results showed more THP-1

immunopurified EVs were sequenced even though approximately same number of vesicles were printed per cell type. Overall, these results demonstrate that embedded droplet 3D printing can enable robust single-EV encapsulation and sequencing, establishing a framework for further adoption and development.

This study developed a 3D printing platform to generate microdroplets suspended in a support medium made from packed micro-organogels, enabling biochemical reactions for sequencing individual EVs. We achieved efficient single EV encapsulation by leveraging Poisson statistics in a dilute EV solution combined with a strategy of close-packing barcoded beads as they passed through the printing nozzle. Our 3D printing platform uniquely combines the droplet production capabilities of microfluidics with the single EV encapsulation and sequencing functionalities of nanoliter microwell approaches. Further, this 3D printing platform enables rapid microdroplet production without the need for complex device fabrication.

In this manuscript we demonstrated how arrays of 3D printed picoliter-sized droplets containing EVs and biochemicals can be used as individual reaction vessels embedded in a support medium. The printed droplets remain stable at the embedded locations during various biochemical reaction conditions, involving multiple thermocycling steps for lysing EVs, capturing and barcoding its nucleic acid contents and retrieving the final products for RNA sequencing library generation. By leveraging the close-packed arrangement of barcoded hydrogel beads, we achieved a 67% loading efficiency of these beads into the printed droplets, with 25% of the droplets encapsulating a single EV. This high loading efficiency is crucial for enhancing the throughput and accuracy of single EV analyses. Similar strategies have been employed in other studies, such as the use of droplet microfluidics to encapsulate individual antibody-DNA labeled EVs into droplets containing barcoded beads, optimizing multiple parameters to achieve efficient encapsulation and subsequent sequencing-based protein analysis of single EVs.²⁸

We utilized commercially available DNA barcoded hydrogel bead technology²⁹ with some modifications. These beads rely on poly(T) capture of poly(A)+ RNAs. The sequencing gel beads were designed such that the oligos on the specific gel bead has a unique barcode to link the reads back to the individual droplet (i.e., an individual cell or EV). Moreover, each of the 109 oligos located on the gel bead has a unique molecular identifier (UMI) to link the reads back to the original RNA transcript. Under these conditions, we identified 3689 unique barcodes (i.e., EVs) with at least two corresponding reads of poly(A)+ RNA sequences per EV from the ~ 3500 THP-1 immunopurified EVs that were printed. Our results are contrasted to those of Wei et al., who used bulk RNA sequencing averages and report 1 copy of mRNA per \sim 10 EVs.³ These authors used ribosomal depletion and did not align their reads to the mitochondrial genome. Our analysis maps several abundantly expressed mitochondrial genes within EVs. In fact, five of the top 10 genes identified in the highly purified THP-1 sample mapped to mitochondrial genes (Table 1).

Although approximately 3,500 ultracentrifugation-purified HEK293T EVs were printed (matching the number of immunopurified THP-1 EVs), bioinformatic analysis identified only 1,099 unique EVs with at least two reads. Several differences are evident between the two data sets. One obvious

difference is that the EVs are derived from different cell types; a head-to-head comparison of the protein cargo of HEK293T and THP-1 cell derived EVs differed significantly. Differences in sequenceable RNA between the two EVs are likely contributed in part to the methods used to purify the EVs. Immunopurification of THP-1 EVs using CD9, CD63, and CD81 antibodies produce a more purified EV population compared to ultracentrifugation. Typically, ultracentrifugation methods isolate higher yields of less pure EVs compared to more precise methods of EV isolation. Ultracentrifugation purification pulls down RNA binding proteins, lipoprotein complexes, additional cellular debris, and nonexosome/EV specific particles that would impact the purity of EVs and thus the RNA sequenced.

Wei, et., showed intact rRNA detectable in large MVs, but not exosomes and RNPs.³ Our sequencing data did not generate any mammalian rRNA reads (Supporting Information for Publication files), which was likely of our study sequencing the RNA content of small EVs. An exception is the presence of mitochondrial 16S rRNA which was more abundant in the affinity purified EVs compared to UC purified EVs (Tables 1 and 2). The MT-RNR2 gene codes for mitochondrial 16S rRNA and may undergo polyadenylation in certain instances.³² The study by Luo et al., ¹² using single EV sequencing of large EV found that 24% rRNA 8% are mitochondrial derived.

A complexity in the EV field is the large number of protocols and different EV isolation methods that will undoubtably contribute to the complexity of the RNA species located within EVs. 33 One of the most comprehensive reports of the RNA diversity located within EVs and their parent cells discovered that human glioma stem cell EVs contained approximately 2% mRNA of the total EV RNA, similar to percentage of mRNA found with total cellular RNA.3 This study identified cytoplasmic rRNA within exosomes, comprising a similar percentage to that found in cellular RNA. By comparison, single cell RNA sequencing typically interrogates the contents of hundreds to a few thousand cells, with UMI-based protocols yielding thousands of mRNA reads per cell. As EVs are up to 200-times smaller than cells, and the fact that RNA is not actively synthesized in EVs, will dramatically reduce their total RNA content compared to their cellular counterparts. While estimates vary based upon cell type, EV isolation technique, particle size, etc., exosomes are reported to contain ~4 attograms of total RNA per vesicle³ or ~1.5 femtograms of protein per EV³³ based on bulk sequencing averages. Moreover, mesenchymal stem cells in culture produced 100 to 600 EVs per cell³⁴ and 1 mL of blood contains 10⁸-10⁹ EVs. 35 This suggests that large numbers of EVs require sequencing to obtain a snapshot of the biology of vesicles and to generate a cumulative number of reads comparable to a typical single cell RNA sequencing experiment.

Our understanding of EV biology, functionality and clinical translation potential is rapidly expanding. However, the complexity of EV composition and cargo, including a paucity of technology to fundamentally address heterogeneity, limits our ability to fully comprehend the potential of this field. The inability to analyze EV nucleic acid content at single vesicle resolution provides a major roadblock to EV-based diagnostics and therapeutic development, and approval from regulatory agencies such as the FDA. There are over 150 completed clinical trials listed on clinicaltrials.gov involving EVs or exosomes as a therapeutic or diagnostic. Analysis of EV preparations at the single vesicle resolution could provide

information on batch-to-batch consistency at higher resolution and help to significantly advance EV drug development in terms of nucleic acid loading amount, uniformity, and reproducibility.

Our 3D printing technology has certain advantages over existing single-vesicle analysis approaches. While digital droplet PCR has unparalleled sensitivity and specificity, it has poor throughput and can only quantify specific nucleic acid entities to which fluorescent probes are designed for known RNA sequences. The 3D printing platform described here is cheaper and faster than most existing single cell and single vesicle analytical approaches and requires less complicated instrumentation; a key innovation is the stable and solid-like medium in which we generate and trap droplets, completely avoiding the many barriers and pitfalls of channel-based microand nanofluidic approaches. Moreover, our approach utilizes commercially available reagents for cDNA synthesis and library generation.

CONCLUSION

Single EV analysis has the power to answer questions regarding their heterogeneity that heretofore are not addressable. It is presently unclear whether the EVs secreted from diseased cells contain selective RNA cargo that results from increased release of EVs with similar RNA content to each other or due to increased RNA packaging within individual EVs. Identifying unique EVs, particularly in the early stages of disease, is difficult because of their scarcity compared to the abundance of EVs shed from healthy cells and tissues. Predictive models suggest that while bulk measurements of the contents of EVs are suited for detecting large tumors (~1 cm³), single EV methods are predicted to distinguish early stage human tumors as small as $1 \times 10_{-5}$ cm³ (~10,000 tumor cells).³⁷ Increasing throughout and combining single EV sequencing methods with purification methods that pull down disease specific EVs will enhance the discovery and implementation of clinical biomarkers.

MATERIALS AND METHODS

Organic Microgel Support Material Formulation. Hydrocarbon-based organic microgels were prepared from the SEP diblock copolymer (molecular weight, 172.6 kg/mol; polydispersity, 1.03), (KRATON G1702); the SEBS triblock copolymer (molecular weight, 98.1 kg/mol; polydispersity, 1.03), (KRATON G1650); and light mineral oil [National Formulary/Food Chemicals Codex (NF/ FCC)-grade] (Fisher Scientific). The organic microgels were prepared in batches of 100 g in a 600 mL beaker. Block copolymer mixtures were prepared at 2.25 wt % diblock copolymer, 2.25 wt % triblock copolymer, and 95.5 wt % light mineral oil. The mixtures were heated to 150 °C and continuously stirred using a Scilogex Overhead Stirrer set to 400 rpm for 4 to 6 h until the disappearance of polymer chunks. The dissolved polymer solution is cooled overnight without stirring; the resulting organic microgel formulation is then centrifuged to remove air bubbles before carefully loading it into the printing chamber for droplet 3D printing.

Droplet 3D Printing Platform. All droplet 3D printing was performed using a custom high-precision 3D printer equipped with three linear translation stages (Newport) with a travel distance of 300 mm in the X-axis and 200 mm in the Y and Z-axis. A linear stage (Physik Instrumente) was attached to the assembled translational stages to act as a syringe pump. Both the syringe pump and translation stages were controlled through MATLAB interface. The aqueous solution to be printed into droplets was loaded into a precision syringe (Hamilton Gastight syringe) fitted with an RN needle and then mounted to the syringe pump. Custom-written MATLAB

functions were used to generate precise trajectory paths for the translation stages and the syringe pump.

The printing chamber used for droplet printing is a custom-built glass bottom rectangular aluminum chamber that fits inside a PCR thermocycler. The frame for the chamber is machined from burrowing a $3'' \times 2''$ aluminum block of 1/4'' thickness, which is then attached to a $3'' \times 2''$ microscope slide (Fisherbrand) using optical glue (Norland). Roughly 5 mL of the organic microgel support material is loaded into the custom-built chamber, which is then used for droplet 3D printing.

Droplet 3D Printing Procedure. To optimize droplet printing protocols, we performed preliminary tests changing various technical printing parameters and measuring the size and number of droplets produced within a given printing run. The technical parameters that were probed for fine-tuning droplet size and control were nozzle translation speed, ν , was varied between 1 and 30 mm/s; volumetric flow rate, Q_i was varied between 1 μ L/h and 300 μ L/h; nozzle radii (inner), R_i was varied between 50 and 375 μ m.

We printed aqueous solutions of 50 μ M rhodamine dispersed with 100 nm polystyrene fluorospheres (FluoSpheres; Invitrogen) at various concentrations as estimated by Poisson's statistics. In these tests, we produced $\sim 10^4$ droplets with varied printing procedures and parameters, enabling the efficient determination of the scaling relationships that control droplet size and spacing. The resulting droplet sizes and fluorosphere encapsulation statistics were quantified with either epifluorescence or confocal fluorescence microscopy and analyzed with custom-written image analysis software.

Biochemical Reaction Protocol in 3D Printed Droplets. Solutions containing $63 \, \mu m$ barcoded DNA hydrogel beads or nonbarcoded practice beads (BDP or FAM-conjugated; RAN Biotechnologies) were loaded into 10, 25, or 50 μ L gastight Hamilton syringes based on the reaction volume. The printing syringes were fitted with a 26s gauge PTFE-coated RN needle to reduce wetting of the aqueous droplets to the needle tip. Reaction mixtures contained EVs $(350 \, \text{EVs}/\bar{\mu}\text{L})$ or $50 \, \text{ng}$ RNA, $0.5 \, \text{mM}$ dNTPs, $5 \, \text{mM}$ DTT, $2.0 \text{ U}/\mu\text{L}$ RNaseOUT, 1× SuperScript IV buffer, $10 \text{ U}/\mu\text{L}$ Super-Script IV reverse transcriptase, and barcoded hydrogel beads at closepacked conditions. Beads were pelleted and supernatant was removed, mixed 1:1 with 2× RT mix, and loaded into a syringe before printing into the custom-built glass bottom chamber containing microgel support medium. Biochemical reaction droplets were printed at a speed of 15 mm/s, acceleration of 10 mm/s², and flow rate of 5 μ L/h. To maximize the printing volume and the yield of the biochemical reaction, the droplets were printed into 10 stacked layers of elliptical spirals with a 150 μ m pitch and spacing.

For single-EV sequencing, 10 μ L of reaction mixture (~3,500 EVs) was printed using the above-mentioned protocol, and the printing chamber was sealed with a transparent PCR film. The sealed chamber was then exposed to 350 nm UV flood lamp (Sunray) for 5 min to release barcoded RT primers. Next, the printing chamber was loaded into the PCR thermocycler (BioRad) fitted with a custom-made 96well aluminum insert with a flat top, during which it was incubated at 50 °C for 2 h (lid at 70 °C) to lyse EVs and perform reverse transcription, followed by enzyme inactivation at 80 °C for 10 min. The support material containing the reaction products was then transferred into microcentrifuge tubes, and the droplets were recovered by centrifugation at 5,000 × g for 15 min at 4 °C, then passed through a 0.45 µm nucleic acid purification column at 16,000 × g for 5 min to remove hydrogel beads. The flow-through was collected for downstream processing. Simulated bulk EV prints were performed using $\sim 10^7$ EVs with barcoded DNA hydrogel beads.

Microscopy Protocols. Micrographs of the droplet arrays of rhodamine solution containing the nanoparticles were imaged using epifluorescence microscopy on an inverted Nikon Eclipse Ti-E microscope using high aperture settings. Micrographs of the fluorescent beads (63 μ m practice beads, RAN Biotechnologies) with either the nanoparticles or EVs were taken using Zeiss LSM 980 confocal microscope using a 60× water immersion objective. Z-stack images of the bottom half of the beads were collected and the

ı

intensity projections of the acquired stacks were used to calculate the EV encapsulation statistics.

Cell Culture. HEK293T and THP-1 cell lines were purchased from ATCC and cultured under standard conditions. Briefly, HEK293T cells were cultured in a complete media consisting of Dulbecco's Modified Eagle's Medium (DMEM) with 10% fetal bovine serum (FBS) and 1× Penicillin—Streptomycin. THP-1 cells were cultured in a complete media consisting of RPMI-1640 with 10% FBS, 0.05 mM 2-mercaptoethanol, and 1× Penicillin—Streptomycin. 24—48 h prior to harvesting EVs from cell culture media, the cells were washed gently with dPBS and replenished in their complete media with EV-depleted FBS. EV-depleted FBS was made by ultracentrifuging FBS at 150,000 × g for 16 h.

EV Isolation. HEK293T and THP-1 EVs were purified using two different techniques, traditional differential ultracentrifugation (HEK293T). Briefly, the supernatant of the 10 min 300 \times g centrifugation step was centrifuged for 30 min at 4 °C and the supernatant was collected. The supernatant of the 3000 × g step was centrifuged at $25,000 \times g$ for 1.5 h and the supernatant was filtered using 0.22 μm filter. The filtered 25,000 \times g supernatant underwent ultracentrifugation on the Beckman Coulter Optima XE-90 at 150,000 × g for 1.5 h. This pellet was carefully washed twice with dPBS and resuspended in dPBS. EVs from THP-1 were purified using immunocapture with magnetic beads coated with antibodies specific to common EV membrane proteins CD63, CD81 and CD9 (NanoPoms) as previously described.³⁹ Briefly, EVs were isolated by a capture-release isolation strategy for EV subtyping via 3Dnanographene immunomagnetic NanoPoms according to manufacturer's protocol.³⁹ Briefly, conditioned cell media were precleaned of cells and cellular debris by two centrifugation steps of 300 × g and 3000 \times g for 10 and 30 min at 4 °C, respectively. NanoPom beads were added to the media and incubated overnight at 4 °C. Photorelease was performed using Analytik-jena UVP 2UV Transilluminator Plus at 365 nm wavelength at 4 °C for 15 min (~6 mW/ cm²). Following purification, EVs suspended in dPBS were freshly used or stored at −80 °C until RNA sequencing is performed. EVs were freshly used or stored at -80 °C until characterization and 3D printing biochemical reactions.

Nanoparticle Tracking Analysis (NTA). Isolated EVs were diluted 500-fold using ion-free dPBS and injected into a Nanosight NS300 or Particle Metrix Zetaview instrument using standard techniques as recommended by the manufacturers. For determining particle concentration, dPBS was run as a blank for background particle concentration.

Cryotransmission Electron Microscopy (Cryo-TEM). Cryo-TEM images of EVs were collected at the University of Florida's ICBR as previously described.³³ The scale bars are 100 nm.

Western Blotting. EV protein was analyzed by Western blot for CD63 (abcam ab68418) using standard techniques. Forty micrograms of total protein extract were resolved on a 4–12% precast SDS-PAGE gel. The resulting membrane was probed with anti-CD63 antibodies overnight at 4 °C followed by incubation with secondary antibody (Anti-rabbit IgG, horseradish peroxidase linked antibody) (Thermo 32460) for 2 h at room temperature. Proteins were detected with ECL reagents and chemiluminescent images were taken on Amersham Imager 680 instrument.

RT-qPCR in Tube and Microgels. Total RNA was extracted from mouse liver tissue, cell pellets, or extracellular vesicles using the miRNeasy Mini Kit (Qiagen) and stored at $-80\,^{\circ}$ C. RNA concentration was measured using a NanoDrop ND-1000 Spectrophotometer (NanoDrop Technologies). For cDNA synthesis, 50–150 ng of total RNA was reverse transcribed using SuperScript IV (ThermoFisher) with one of the following primers: random hexamers, oligo $(dT)_{12-18}$, RAN Biotechnologies RT oligo mimics (IDT), or stem-loop primers (ThermoFisher). Detailed RT conditions are described in the 3D Printing for Biochemical Reactions in Droplets section. For 3D printing experiments, 250 ng of Luciferase mRNA was printed alongside an oligo(dT) RT primer. Resulting cDNA (1:30 dilution) was quantified by qPCR using TaqMan assays (ThermoFisher) for miRNA/U6 or PowerTrack SYBR Green Master Mix

(ThermoFisher) with custom mRNA primers on a QuantStudio 7 Flex System. Primer sequences are listed in Supporting Information for Publication file.

To optimize EV heat lysis for reverse transcription, 10⁷ EVs were incubated in 5X RT buffer at the target lysis temperature for 5 min, then placed on ice. For lysis temperatures ≥50 °C, RT was performed at 50 °C for 2 h, followed by enzyme inactivation at 80 °C for 10 min and hold at 4 °C. For lysis temperatures <50 °C, RT was conducted at 37 °C for 2 h, followed by the same inactivation and hold steps. Onestep RT-PCR in 3D-printed droplets was performed using the OneTaq RT-PCR Kit (NEB, E5310S) with 150 ng DNase-treated liver RNA, 18S primers, and 1× SYBR Green. Droplets were thermocycled in a microgel-filled aluminum chamber. SYBR fluorescence was imaged using epifluorescence microscopy at 20× magnification, and 18S PCR products were recovered by centrifugation and analyzed via electrophoresis on a 1.5% agarose gel.

Luciferase mRNA 3D Printing and Sequencing. Codonoptimized firefly luciferase mRNA (TriLink Biotechnologies; 1929 nt) was fully substituted with 5-methoxyuridine, CleanCap AG-capped, and polyadenylated (120A), and included proprietary 5' and 3' UTRs. For reverse transcription, 50 ng of luciferase mRNA was used as described in the 3D Printing section described previously. Closepacked barcoded beads were mixed 1:1 with 2× reverse transcription components to generate a 1× final reaction mixture, which was loaded into a 50 µL Hamilton syringe and 3D printed into the printing chamber containing microgel support medium. The printing chamber was incubated at 50 °C for 2 h to capture poly(A)+ RNA and perform reverse transcription, followed by enzyme inactivation at 80 °C for 10 min.

3D Printing RNA Sequencing Library Preparation and RNA Sequencing. An adapted inDrop-seq protocol based on Zilionis et was used, compatible with all Illumina next-generation sequencing (NGS) platforms. Library preparation began with enzymatic cleanup of reverse-transcribed cDNA using Exonuclease I $(1 \text{ U}/\mu\text{L}; \text{ Thermo Scientific, EN0581})$ to remove unused singlestranded primers, and HinfI (1 U/ μ L; Thermo Scientific, FD0804) to cleave double-stranded DNA, both in 1× FastDigest buffer at 37 °C for 30 min. The cDNA was purified using 1.5× AMPure XP beads (Beckman Coulter, A63880) and eluted in 17 µL of nuclease-free water. Double-stranded DNA synthesis was carried out in a 20 μ L reaction using the NEBNext mRNA Second Strand Synthesis Kit (NEB, E6111S) at 16 °C for 2.5 h followed by 65 °C for 20 min. Amplification via in vitro transcription (IVT) was performed overnight (15 h at 37 °C) using the HiScribe T7 High Yield RNA Synthesis Kit (NEB, E2040S), and purified with 1.3× AMPure XP beads.

The amplified RNA (aRNA) was fragmented at 70 °C for 2 min using zinc-catalyzed cleavage (Invitrogen, AM8740). Fragmented aRNA was reverse transcribed using a random hexamer PE2-N6 primer to introduce the PE2 hybridization site. The mixture, containing dNTPs (500 μ M each) and PE2-N6 primer (10 μ M), was incubated at 70 °C for 3 min, chilled on ice, then subjected to reverse transcription at 30 °C for 10 min, 42 °C for 1 h, and 70 °C for enzyme inactivation. The RT reaction included 1× PrimeScript buffer, RNaseOUT (2 U/ μ L), and PrimeScript Reverse Transcriptase (5 U/ μ L; Takara, 2680A). The final product was purified using 1.2× AMPure XP beads. To determine the optimal number of PCR amplification cycles, qPCR was performed using the formula: 2 + $(C_t - 4.25)$, where $4.25 = \log_2(19)$, accounting for the 19-fold higher library input relative to diagnostic PCR. Amplification was carried out using KAPA HiFi HotStart ReadyMix (Roche, 50-196-5217) with the following cycling conditions: 98 °C for 2 min; 2 cycles of 98 °C for 20 s, 55 $^{\circ}$ C for 30 s, 72 $^{\circ}$ C for 40 s; X cycles of 98 $^{\circ}$ C for 20 s, 65 $^{\circ}$ C for 30 s, 72 $^{\circ}$ C for 40 s; final extension at 72 $^{\circ}$ C for 5 min.

Libraries were purified using 0.7X AMPure XP beads and stored at -20 °C. PE1 primers (with 6-bp sample indices) and PE2 primers were added during final PCR for multiplexing. Final libraries were pooled at 1.0 nM and sequenced on an Illumina NovaSeq 6000 S4 flow cell with the following read structure: 61 cycles for Read 1, 6 cycles for the index, and 51 cycles for Read 2. PhiX was spiked in at 10% as a control. Sequencing yielded >2.5 billion reads per lane, with ≥80% of bases at Q30 or above. Sequencing was performed at the University of Florida Interdisciplinary Center for Biotechnology Research (ICBR).

Statistical and Bioinformatic Analysis. First, verification of sequencing experiment production of high-quality data was done by canonical summary statistics used in RNA-seq bioinformatics pipelines. This included the read length distribution, mapping quality scores, and GC content, among others. Verification that reads captured were poly(A)+ RNAs rather than poly(A)- RNAs and genome mapping was then performed. EVs with low-quality reads were excluded from further analysis, and the experimental procedure was adjusted if they comprise a significant fraction of sequenced EVs. After the primary quality control is satisfactorily completed, we proceeded to the "preprocessing" steps. The most notable aspects of this are exploratory analyses of the single EV data set to understand fundamental properties such as the total read and expressed gene counts per EV. As the valid barcode sequences were known, barcoded read preprocessing included a step to confirm that reads had a valid barcode or were within 2 mismatches of a valid barcode if it would yield an unambiguous match. Additionally, we used a filtering step to remove reads if they had barcodes with counts below a specified threshold of 50 for abundantly expressed luciferase gene and 5 for EV samples. Finally, read alignment allowed for a small number of mismatches to the reference transcripts. Examination of summary statistics such as these allowed us to tell apart singlets from multiplets, though more sophisticated techniques designed for scRNA-seq data were employed when necessary.⁴⁰ Beyond comparison of summary statistics, we assessed our sequencing results by examining the genelevel correlation between our single EV and between pairs of single

ASSOCIATED CONTENT

Supporting Information

The Supporting Information is available free of charge at https://pubs.acs.org/doi/10.1021/acsami.5c09959.

Experimental setup and details of 3D printing and biochemical reactions in droplet; RNA sequencing library preparation details; list of oligonucleotides and primer sequences; single EV in droplet and DNA barcode schematics; EV characterization; single EV RNA sequencing library quality control; additional biochemical reactions printed and in-tube controls; reads and genes per EV statistics; and genes per EV analysis (PDF)

Sequences mapping, annotated regions, and EVs (XLSX)

AUTHOR INFORMATION

Corresponding Authors

Thomas E. Angelini – Department of Physics, College of Liberal Arts and Sciences, University of Florida, Gainesville, Florida 32611, United States; o orcid.org/0000-0002-0313-4341; Email: t.e.angelini@ufl.edu

Thomas D. Schmittgen – Department of Pharmaceutics, College of Pharmacy, University of Florida, Gainesville, Florida 32610, United States; oorcid.org/0000-0002-2812-8546; Email: tschmittgen@ufl.edu

Authors

Andrew A. Brock - Department of Pharmaceutics, College of Pharmacy, University of Florida, Gainesville, Florida 32610, United States

Senthilkumar Duraivel - Department of Materials Science and Engineering, Cornell University, Ithaca, New York 14850, United States

- Jinmai Jiang Department of Pharmaceutics, College of Pharmacy, University of Florida, Gainesville, Florida 32610, United States
- Jonathan Fischer Department of Biostatistics, College of Public Health and Health Professions, University of Florida, Gainesville, Florida 32603, United States
- Zachary F. Greenberg Department of Pharmaceutics, College of Pharmacy, University of Florida, Gainesville, Florida 32610, United States; orcid.org/0000-0001-9626-2694
- Mei He Department of Pharmaceutics, College of Pharmacy, University of Florida, Gainesville, Florida 32610, United States; orcid.org/0000-0001-5316-9326

Complete contact information is available at: https://pubs.acs.org/10.1021/acsami.5c09959

Author Contributions

[‡]A.B. and S.D. contributed equally to this paper.

Notes

The authors declare the following competing financial interest(s): Andrew A. Brock, Jinmai Jiang, Thomas E. Angelini, and Thomas D. Schmittgen are cofounders of DREAMHIT Bio LLC. Andrew A. Brock, Senthilkumar Duraivel, Jinmai Jiang, Thomas E. Angelini, and Thomas D. Schmittgen hold patents related to the research. All other authors declare no conflicts of interest.

ABBREVIATIONS

RT = reverse transcription/reverse transcriptase

EV = extracellular vesicle

UC = ultracentrifugation

NTC = no template control

MV = microvesicles

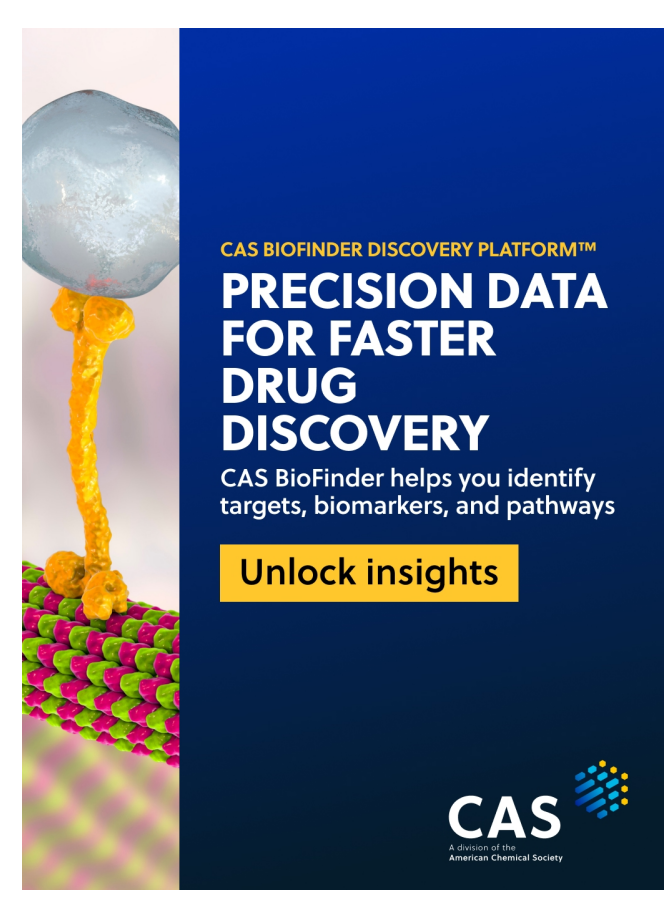
REFERENCES

- (1) Yang, S.; Zhang, L.; Purohit, V.; Shukla, S. K.; Chen, X.; Yu, F.; Fu, K.; Chen, Y.; Solheim, J.; Singh, P. K.; Song, W.; Dong, J. Active YAP promotes pancreatic cancer cell motility, invasion and tumorigenesis in a mitotic phosphorylation-dependent manner through LPAR3. *Oncotarget* **2015**, *6* (34), 36019–31.
- (2) Rodosthenous, R. S.; Hutchins, E.; Reiman, R.; Yeri, A. S.; Srinivasan, S.; Whitsett, T. G.; Ghiran, I.; Silverman, M. G.; Laurent, L. C.; Van Keuren-Jensen, K.; Das, S. Profiling Extracellular Long RNA Transcriptome in Human Plasma and Extracellular Vesicles for Biomarker Discovery. *iScience* 2020, 23 (6), No. 101182.
- (3) Wei, Z.; Batagov, A. O.; Schinelli, S.; Wang, J.; Wang, Y.; El Fatimy, R.; Rabinovsky, R.; Balaj, L.; Chen, C. C.; Hochberg, F.; Carter, B.; Breakefield, X. O.; Krichevsky, A. M. Coding and noncoding landscape of extracellular RNA released by human glioma stem cells. *Nat. Commun.* 2017, 8 (1), 1145.
- (4) Valadi, H.; Ekstrom, K.; Bossios, A.; Sjostrand, M.; Lee, J. J.; Lotvall, J. O. Exosome-mediated transfer of mRNAs and microRNAs is a novel mechanism of genetic exchange between cells. *Nat. Cell Biol.* **2007**, *9* (6), 654–9.
- (5) Morales, R. T.; Ko, J. Future of Digital Assays to Resolve Clinical Heterogeneity of Single Extracellular Vesicles. *ACS Nano* **2022**, *16* (8), 11619–11645.
- (6) Bordanaba-Florit, G.; Royo, F.; Kruglik, S. G.; Falcon-Perez, J. M. Using single-vesicle technologies to unravel the heterogeneity of extracellular vesicles. *Nat. Protoc* **2021**, *16* (7), 3163–3185.
- (7) Smith, Z. J.; Lee, C.; Rojalin, T.; Carney, R. P.; Hazari, S.; Knudson, A.; Lam, K.; Saari, H.; Ibanez, E. L.; Viitala, T.; Laaksonen, T.; Yliperttula, M.; Wachsmann-Hogiu, S. Single exosome study reveals subpopulations distributed among cell lines with variability related to membrane content. *J. Extracell. Vesicles* **2015**, *4*, No. 28533.

- (8) Carney, R. P.; Hazari, S.; Colquhoun, M.; Tran, D.; Hwang, B.; Mulligan, M. S.; Bryers, J. D.; Girda, E.; Leiserowitz, G. S.; Smith, Z. J.; Lam, K. S. Multispectral Optical Tweezers for Biochemical Fingerprinting of CD9-Positive Exosome Subpopulations. *Anal. Chem.* **2017**, 89 (10), 5357–5363.
- (9) Zhang, H.; Freitas, D.; Kim, H. S.; Fabijanic, K.; Li, Z.; Chen, H.; Mark, M. T.; Molina, H.; Martin, A. B.; Bojmar, L.; Fang, J.; Rampersaud, S.; Hoshino, A.; Matei, I.; Kenific, C. M.; Nakajima, M.; Mutvei, A. P.; Sansone, P.; Buehring, W.; Wang, H.; et al. Identification of distinct nanoparticles and subsets of extracellular vesicles by asymmetric flow field-flow fractionation. *Nat. Cell Biol.* **2018**, *20* (3), 332–343.
- (10) Lee, K.; Fraser, K.; Ghaddar, B.; Yang, K.; Kim, E.; Balaj, L.; Chiocca, E. A.; Breakefield, X. O.; Lee, H.; Weissleder, R. Multiplexed Profiling of Single Extracellular Vesicles. *ACS Nano* **2018**, *12* (1), 494–503.
- (11) Wu, D.; Yan, J.; Shen, X.; Sun, Y.; Thulin, M.; Cai, Y.; Wik, L.; Shen, Q.; Oelrich, J.; Qian, X.; Dubois, K. L.; Ronquist, K. G.; Nilsson, M.; Landegren, U.; Kamali-Moghaddam, M. Profiling surface proteins on individual exosomes using a proximity barcoding assay. *Nat. Commun.* **2019**, *10* (1), 3854.
- (12) Luo, T.; Chen, S. Y.; Qiu, Z. X.; Miao, Y. R.; Ding, Y.; Pan, X. Y.; Li, Y.; Lei, Q.; Guo, A. Y. Transcriptomic Features in a Single Extracellular Vesicle via Single-Cell RNA Sequencing. *Small Methods* **2022**, *6* (11), No. e2200881.
- (13) Collins, D. J.; Neild, A.; deMello, A.; Liu, A. Q.; Ai, Y. The Poisson distribution and beyond: methods for microfluidic droplet production and single cell encapsulation. *Lab Chip* **2015**, *15* (17), 3439–59.
- (14) Brouzes, E.; Kruse, T.; Kimmerling, R.; Strey, H. H. Rapid and continuous magnetic separation in droplet microfluidic devices. *Lab Chip* **2015**, *15* (3), 908–19.
- (15) Ko, J.; Bhagwat, N.; Yee, S. S.; Ortiz, N.; Sahmoud, A.; Black, T.; Aiello, N. M.; McKenzie, L.; O'Hara, M.; Redlinger, C.; Romeo, J.; Carpenter, E. L.; Stanger, B. Z.; Issadore, D. Combining Machine Learning and Nanofluidic Technology To Diagnose Pancreatic Cancer Using Exosomes. ACS Nano 2017, 11 (11), 11182–11193.
- (16) Gruner, P.; Riechers, B.; Orellana, L. A. C.; Brosseau, Q.; Maes, F.; Beneyton, T.; Pekin, D.; Baret, J. C. Stabilisers for water-influorinated-oil dispersions: Key properties for microfluidic applications. *Curr. Opin. Colloid Interface Sci.* **2015**, 20 (3), 183–191.
- (17) Bhattacharjee, T.; Gil, C. J.; Marshall, S. L.; Urueña, J. M.; O'Bryan, C. S.; Carstens, M.; Keselowsky, B.; Palmer, G. D.; Ghivizzani, S.; Gibbs, C. P.; Sawyer, W. G.; Angelini, T. E. Liquid-like Solids Support Cells in 3D. ACS Biomaterials Science and Engineering 2016, 2 (10), 1787–1795.
- (18) Bhattacharjee, T.; Zehnder, S. M.; Rowe, K. G.; Jain, S.; Nixon, R. M.; Sawyer, W. G.; Angelini, T. E. Writing in the granular gel medium. *Sci. Adv.* **2015**, *1* (8), No. e1500655.
- (19) Duraivel, S.; Laurent, D.; Rajon, D. A.; Scheutz, G. M.; Shetty, A. M.; Sumerlin, B. S.; Banks, S. A.; Bova, F. J.; Angelini, T. E. A silicone-based support material eliminates interfacial instabilities in 3D silicone printing. *Science* **2023**, *379* (6638), 1248–1252.
- (20) O'Bryan, C. S.; Bhattacharjee, T.; Hart, S.; Kabb, C. P.; Schulze, K. D.; Chilakala, I.; Sumerlin, B. S.; Sawyer, W. G.; Angelini, T. E. Self-assembled micro-organogels for 3D printing silicone structures. *Sci. Adv.* **2017**, *3* (5), No. e1602800.
- (21) Morley, C. D.; Flores, C. T.; Drake, J. A.; Moore, G. L.; Mitchell, D. A.; Angelini, T. E. Spatiotemporal T cell dynamics in a 3D bioprinted immunotherapy model. *Bioprinting* **2022**, 28, No. e00231.
- (22) Clausell-Tormos, J.; Lieber, D.; Baret, J. C.; El-Harrak, A.; Miller, O. J.; Frenz, L.; Blouwolff, J.; Humphry, K. J.; Koster, S.; Duan, H.; Holtze, C.; Weitz, D. A.; Griffiths, A. D.; Merten, C. A. Droplet-based microfluidic platforms for the encapsulation and screening of Mammalian cells and multicellular organisms. *Chem. Biol.* **2008**, *15* (5), 427–37.

- (23) Edd, J. F.; Di Carlo, D.; Humphry, K. J.; Koster, S.; Irimia, D.; Weitz, D. A.; Toner, M. Controlled encapsulation of single-cells into monodisperse picolitre drops. *Lab Chip* **2008**, *8* (8), 1262–4.
- (24) Tumarkin, E.; Tzadu, L.; Csaszar, E.; Seo, M.; Zhang, H.; Lee, A.; Peerani, R.; Purpura, K.; Zandstra, P. W.; Kumacheva, E. Highthroughput combinatorial cell co-culture using microfluidics. *Integr Biol.* (*Camb*) **2011**, 3 (6), 653–62.
- (25) Abate, A. R.; Chen, C. H.; Agresti, J. J.; Weitz, D. A. Beating Poisson encapsulation statistics using close-packed ordering. *Lab Chip* **2009**, *9* (18), 2628–31.
- (26) Thery, C.; Witwer, K. W.; Aikawa, E.; Alcaraz, M. J.; Anderson, J. D.; Andriantsitohaina, R.; Antoniou, A.; Arab, T.; Archer, F.; Atkin-Smith, G. K.; Ayre, D. C.; Bach, J. M.; Bachurski, D.; Baharvand, H.; Balaj, L.; Baldacchino, S.; Bauer, N. N.; Baxter, A. A.; Bebawy, M.; Beckham, C.; et al. Minimal information for studies of extracellular vesicles 2018 (MISEV2018): a position statement of the International Society for Extracellular Vesicles and update of the MISEV2014 guidelines. *J. Extracell. Vesicles* 2018, 7 (1), No. 1535750.
- (27) Wang, X.; Weidling, I.; Koppel, S.; Menta, B.; Perez Ortiz, J.; Kalani, A.; Wilkins, H. M.; Swerdlow, R. H. Detection of mitochondria-pertinent components in exosomes. *Mitochondrion* **2020**, *55*, 100–110.
- (28) Ko, J.; Wang, Y.; Sheng, K.; Weitz, D. A.; Weissleder, R. Sequencing-Based Protein Analysis of Single Extracellular Vesicles. *ACS Nano* **2021**, *15* (3), 5631–5638.
- (29) Zilionis, R.; Nainys, J.; Veres, A.; Savova, V.; Zemmour, D.; Klein, A. M.; Mazutis, L. Single-cell barcoding and sequencing using droplet microfluidics. *Nat. Protoc* **2017**, *12* (1), 44–73.
- (30) Burbidge, K.; Zwikelmaier, V.; Cook, B.; Long, M. M.; Balva, B.; Lonigro, M.; Ispas, G.; Rademacher, D. J.; Campbell, E. M. Cargo and cell-specific differences in extracellular vesicle populations identified by multiplexed immunofluorescent analysis. *J. Extracell. Vesicles* **2020**, *9* (1), No. 1789326.
- (31) An, M.; Wu, J.; Zhu, J.; Lubman, D. M. Comparison of an Optimized Ultracentrifugation Method versus Size-Exclusion Chromatography for Isolation of Exosomes from Human Serum. *J. Proteome Res.* **2018**, *17* (10), 3599–3605.
- (32) Pearce, S. F.; Rorbach, J.; Van Haute, L.; D'Souza, A. R.; Rebelo-Guiomar, P.; Powell, C. A.; Brierley, I.; Firth, A. E.; Minczuk, M. Maturation of selected human mitochondrial tRNAs requires deadenylation. *eLife* **2017**, *6*, e27596.
- (33) Sutaria, D. S.; Jiang, J.; Elgamal, O. A.; Pomeroy, S. M.; Badawi, M.; Zhu, X.; Pavlovicz, R.; Azevedo-Pouly, A. C. P.; Chalmers, J.; Li, C.; Phelps, M. A.; Schmittgen, T. D. Low active loading of cargo into engineered extracellular vesicles results in inefficient miRNA mimic delivery. *J. Extracell. Vesicles* **2017**, *6* (1), No. 1333882.
- (34) Haraszti, R. A.; Miller, R.; Stoppato, M.; Sere, Y. Y.; Coles, A.; Didiot, M. C.; Wollacott, R.; Sapp, E.; Dubuke, M. L.; Li, X.; Shaffer, S. A.; DiFiglia, M.; Wang, Y.; Aronin, N.; Khvorova, A. Exosomes Produced from 3D Cultures of MSCs by Tangential Flow Filtration Show Higher Yield and Improved Activity. *Mol. Ther* **2018**, *26* (12), 2838–2847.
- (35) Huang, X.; Yuan, T.; Tschannen, M.; Sun, Z.; Jacob, H.; Du, M.; Liang, M.; Dittmar, R. L.; Liu, Y.; Liang, M.; Kohli, M.; Thibodeau, S. N.; Boardman, L.; Wang, L. Characterization of human plasma-derived exosomal RNAs by deep sequencing. *BMC Genomics* **2013**, *14*, 319.
- (36) Zhang, P.; Zhou, X.; He, M.; Shang, Y.; Tetlow, A. L.; Godwin, A. K.; Zeng, Y. Ultrasensitive detection of circulating exosomes with a 3D-nanopatterned microfluidic chip. *Nature Biomedical Engineering* 2019, 3, 438
- (37) Ferguson, S.; Weissleder, R. Modeling EV Kinetics for Use in Early Cancer Detection. *Adv. Biosyst.* **2020**, *4* (12), No. e1900305.
- (38) Thery, C.; Amigorena, S.; Raposo, G.; Clayton, A. Isolation and characterization of exosomes from cell culture supernatants and biological fluids. *Curr. Protoc. Cell Biol.* **2006**, *30*, *3.22.1*.
- (39) He, N.; Thippabhotla, S.; Zhong, C.; Greenberg, Z.; Xu, L.; Pessetto, Z.; Godwin, A. K.; Zeng, Y.; He, M. Nano pom-poms

- prepared exosomes enable highly specific cancer biomarker detection. Commun. Biol. 2022, 5 (1), 660.
- (40) Wolock, S. L.; Lopez, R.; Klein, A. M. Scrublet: Computational Identification of Cell Doublets in Single-Cell Transcriptomic Data. *Cell Syst* **2019**, *8* (4), 281–291.



Supporting Information

RNA Sequencing at Single Vesicle Resolution via 3D Printed Embedded Droplet Arrays

Andrew A. Brock^{1, ‡}, Senthilkumar Duraivel^{2, ‡}, Jinmai Jiang¹, Jonathan Fischer³, Zachary

F. Greenberg¹, Mei He¹, Thomas E. Angelini ^{4, *} and Thomas D. Schmittgen^{1, *}

¹Department of Pharmaceutics, College of Pharmacy, University of Florida, Gainesville, FL, 32610, USA

²Department of Materials Science and Engineering, Herbert Wertheim College of Engineering, University of Florida, Gainesville, FL 32611, USA

³Department of Biostatistics, College of Public Health and Health Professions, University of Florida, Gainesville, FL, 32603, USA

⁴Department of Mechanical and Aerospace Engineering, Herbert Wertheim College of Engineering, University of Florida, Gainesville, FL 32611, USA

‡A.B. and S.D. contributed equally to this paper.

*Corresponding author: Thomas E. Angelini, <u>t.e.angelini@ufl.edu</u>, Thomas D. Schmittgen, <u>tschmittgen@ufl.edu</u>

Supplemental Materials and Methods

3D Printing for Biochemical Reactions in Droplets

All droplet printing was performed using a custom built high-precision 3D printer, containing three linear translational stages (Newport) with a travel distance of 300 mm in the X-axis and 200 mm in the Y and Z-axis. A linear stage (Physik Instrumente) was attached to the assembled translational stages to act as a syringe pump. Both the syringe pump and translation stages were controlled through custom-written MATLAB script functions and trajectory files. Aqueous solutions used for droplet generation were loaded into 10, 25, or 50 µL gastight syringes (Hamilton). Barcoded DNA hydrogel beads, indrop seq, are 63 µm microspheres with 109 barcoded DNA oligos (RAN Biotechnologies). The practice beads are identical to those containing barcoded DNA oligos used for the RNA sequencing except they are BDP or FAM-conjugated and do not contain the oligos (RAN Biotechnologies). For EV encapsulation and biochemical reaction droplet printing tests, the syringes were equipped with an RN needle of desired gauge sizes in the ranges of 26s to 32 gauge sizes based on the targeted droplet sizes. For biochemical reactions syringes were loaded with solutions containing 63 µm barcoded DNA oligos or fluorescent beads dispersed with EVs, the droplets were printed at a speed of 15 mm/sec and an acceleration of 10 mm/sec² at a flow rate of 5 μL/h into 10 elliptical spirals of 150 μm pitch, with 10 stacks on top of each other with a layer spacing of 150 µm using a 26s gauge RN needle. To perform biochemical reactions with barcoded DNA hydrogel beads, a 10 µl master mix of EVs (350 EVs/µL) or 50 ng of total RNA, dNTPs (0.5 mM each; Applied Biosystems[™], cat. no. N8080261), DTT (5 mM), RNaseOUT RNase inhibitor (2.0 U/μL; Invitrogen, cat. no. 10777019), Superscript IV reaction buffer (1X) and Superscript IV thermostable reverse transcriptase (10 U/µL; Invitrogen cat. no. 18090050) was prepared. Simulated bulk EV prints with barcoded DNA hydrogel beads were performed with approximately

10⁷ EVs. In a separate 200 μL reaction tubes, add the 5 μL of packed barcoded hydrogel beads (10⁶ beads per mL) and then briefly microcentrifuge the tube. Carefully remove the supernatant being careful not to disturb the bead pellet and briefly centrifuge to remove any residual supernatant. Resuspend the packed beads (1:1) with 10 µL of the 2X reverse transcription reaction components to make final 10 µL, 1X reaction volume. The final solution is loaded into a 10, 25, or 50 µL Hamilton syringe depending upon total reaction volume. To load the 10 µL of the 1X reaction buffer into a 10 µL Hamilton syringe, first plunge the syringe several times with air. Then remove the plunger from the syringe. Carefully load a P-20 micropipette the final reaction mixture and from the top of the syringe carefully place pipette tip into the syringe opening and slowly and gently dispense the reaction into the syringe being careful to introduce and air bubbles into the syringe (i.e. do not dispense past the first stop on the pipette). Slowly add the plunger into the syringe being careful not to dispense any liquid from the syringe. Next the syringe is attached to the 3D printing apparatus and 3D printed into the custom-made printing chamber containing roughly 5 mL of the microgel support medium and all 10 μL is 3D printed as described above. Once printed, the printing chamber is sealed with a MicroAmp optical adhesive film (Thermo) and the barcoded RT primers are released from the beads by exposure to 350 nm UV light box for 5 minutes. The printing chamber is transferred to the thermocycler (BioRad) fitted with a custom made 96-well flat top aluminum insert for incubation at 50° C for 2 hours to lyse the EVs and perform reverse transcription (lid temperature set to 70° C) and then Superscript IV RT is inactivated at 80° C for 10 minutes. The microgel is transferred to multiple 2 mL round bottom microcentrifuge tubes and then 5 µL of molecular biology grade water is added to the organogel. The microcentrifuge tubes are centrifugation at 5000 xg for 15 min at 4° C to separate the aqueous reaction from the organogel. To remove the hydrogel beads form the cDNA solution ~25 μL of aqueous cDNA is pipetted into a nucleic acid purification column (pore size $0.45 \mu m$) that was pre-wetted with $10 \mu L$ of molecular biology grade water. Centrifuge for 5 minutes at 16,000 xg (4° C) into a 1.5-ml DNA LoBind tube to collect the cDNA.

Estimating EV concentration for single EV encapsulation

To optimize the concentration of EVs required to achieve the statistical distribution required for single EV encapsulation per droplet, we performed tests using fluorospheres in place of EVs. The fluorosphere concentrations were chosen by following the Poisson distribution, given by $p(k,\lambda) = \lambda^k e^{-\lambda}/k!$, where p is the probability of finding k particles in a droplet for a sample concentration of λ particles per sample volume. For a target droplet size, the fluorosphere concentrations were made at varying λ until 5% of droplets contain k > 1 and 98% of these droplets contain k = 1 particle. For example, to print droplets using the previous protocol of 100 μ m diameter, such that only 0.98 x 0.05 of the droplet population has 1 fluorosphere, the required fluorosphere concentration can be estimated from the Poisson distribution to be roughly 150 particles per microliter.

RT-qPCR in tube and microgels

Total RNA was extracted from mouse liver tissue, cell pellets, or EVs using the miRNeasy Mini Kit (Qiagen) per the manufacturer's instructions. Purified RNA was stored at -80° C until use. RNA concentration was determined using a ND-1000 Spectrophotometer (Nanodrop Technologies). 50 – 150 ng of total RNA was reverse transcribed with SuperScript IV RT ³⁶ using random hexamers, oligo(dT) 12-18 primer, RAN Biotechnologies RT oligo mimic (IDT), or stem loop primers to mature miRNAs and U6 (ThermoFisher) to generate cDNA for mRNA, microRNA, and U6 detection, respectively. Detailed RT reaction components and conditions are

outlined in 3D Printing Protocols methods section. 3D printings with luciferase mRNA and oligo(dT) RT primer used 250 ng of mRNA. cDNA was diluted 1:30 and quantified by qPCR using Taqman Assays to miRNA or U6 targets (ThermoFisher), PowerTrack SYBR green master mix (ThermoFisher) and in-house designed qPCR primers (2 μM) to mRNA on a QuantStudioTM 7 Flex Real-Time PCR System (Applied Biosystems). In reactions to optimize heat lysis of EVs for reverse transcription reactions, 10⁷ EVs were incubated with 5X First Strand Synthesis reverse transcription buffer at listed lysis temperature for 5 minutes and then placed on ice prior to the addition of the rest of reverse transcription reagents. Following exposure of EVs to lysis temperatures at or above 50°C, similar thermocycler temperature cycles were followed: 50°C for 2 hours, 80°C for 10 minutes, and 4°C until cDNA storage at -20°C. For lysis temperatures below 50°C RT was performed at 37°C for 2 hours, followed by 80°C for 10 minutes, and 4°C until cDNA storage at -20°C. qPCR primer sequences are provided in the supplemental material below. To perform biochemical reactions in droplets printed via 3D printing technique to perform one step RT-PCR, OneTag® RT-PCR Kit (NEB, cat. no. E5310S) is used (per manufacturer's instructions). 150 ng of DNased mouse liver total RNA, 18S PCR primers, and 1X SYBR green was printed and microgel aluminum chamber was placed in the thermocycler for a one-step RT-PCR. Epifluorescence microscopy at 20X magnification was used to detect SYBR green bound DNA in the microgel. The PCR product was isolated from the microgel with centrifugation (15 minutes at 5000 xg) and resolved on an 1.5 % agarose gel to analyze the 18S PCR product.

3D Printing RNA Sequencing Library Preparation and RNA Sequencing

The next-generation sequencing strategy used in our protocol, inDrop seq, is designed to work with all Illumina sequencing platforms and follows that developed in Zilionis et al.²⁵, with some modifications. The detailed steps of library preparation begin with an enzymatic cleanup reaction

of the reverse transcription reaction cDNA product. 3'-5' exonuclease ExoI (1 U/μL; Thermo Scientific, cat. no. EN0581) is used to digest unused ssDNA primers along with the dsDNAspecific restriction endonuclease by HinfI (1 U/µL, Thermo Scientific, cat. no. FD0804), in 10X FastDigest buffer via a 30-minute digestion at 37°C. AMPure XP sample purification beads (1.5X, Beckman Coulter, cat. no. A63880) are used to purify the library and the sample is eluted in 17 μL of nuclease free water. A 20 µL second-strand synthesis reaction with NEBNext mRNA Second Strand Synthesis kit (NEB, cat. no. E6111S) is used to generate dsDNA under the thermocycler conditions: 16°C for 2.5 hours and 20 min at 65°C. An overnight in vitro transcription (IVT) reaction with HiScribe T7 High Yield RNA synthesis kit (NEB, cat. no. E2040S) amplifies the double stranded cDNA library following incubation at 37°C for 15 hours on a thermocycler with the lid temperature set to 50°C. Libraries are cleaned up with AMPure XP sample purification beads (1.3X). The resulting amplified RNA (aRNA) is fragmented by zinc-ion-catalyzed cleavage (Invitrogen, cat. no. AM8740) for 2 minutes at 70°C. A second reverse transcription reaction followed by limited-cycle PCR is used to convert the aRNA into a dsDNA library with P5 and P7 Illumina capture and primer sites to be compatible with Illumina sequencing platforms. This RT reaction uses a random hexamer PE2-N6 RT primer to introduce PE2 PCR hybridization start site. Purified fragmented RNA is incubated with dNTPs (500 μM, each) and the PE2-N6 primer (10 μM) at 70°C for 3 minutes, placed on ice and PrimeScript buffer (1X), RNase OUT (2 U/μL), and PrimeScript reverse transcriptase (5 U/μL; Takara, cat. no. 2680A) is added. The thermocycler conditions are as follows: 30°C for 10 minutes, 42°C for 1 hour, and 70°C enzyme inactivation. The RT product is purified with AMPure XP sample purification beads 1.2X. Quantitation to determine the correct number of cycles for PCR amplification to generate a completed library were done by SYBR Green detection qPCR and the formula $[2+(C_T-4.25)]$ if the library input is 19 times

higher than the diagnostic PCR (log₂19=4.25). Kapa HiFi HotStart (Roche, cat. no. 50-196-5217) diagnostic and library PCR conditions are as follows: cycle 1-98°C for 2 min; cycle 2 and 3-98°C for 20 seconds, 55°C for 30 seconds, and 72°C for 40s; cycle 4 through X 98°C for 20 seconds, 65°C for 30 seconds, and 72°C for 40s; and a final extension at 72°C for 5 minutes. PE1 and PE2 primer mix are used at a final concentration of 5 µM. The final library is purified with an AMPure XP sample purification bead cleanup (0.7X) and stored at -20°C until RNA sequencing. A sample index (6 bp Library Index in sequencing primer) is added during the final PCR to allow pooling of multiple libraries for multiplexed sequencing in a single run by using different PE1/PE2 primer mix variants to introduce unique Illumina library indices per each sample. Individual samples were pooled and the "working pool" was used as input in the NovaSeq6000 instrument using sample preparation protocol. A final loading concentration of 1.0 nM library resulted in the best balance between sequencing data yield and quality. Under these conditions, 61 cycles for Read 1, 6 cycles for sample index, and 51 cycles for Read 2 run on a NovaSeq 6000 S4 flow cell generates >2.5 billion reads/lane with ≥ 80% of bases higher than Q30. PhiX was spiked into the final pooled RNA sequencing library at 10%. Sequencing was performed at University of Florida Interdisciplinary Center for Biotechnology Research (ICBR).

LIST OF SEQUENCES

In house qPCR primer designs:

18S:

Sense: 5'- GTAACCCGTTGAACCCCATT -3'

Antisense: 5'- CCATCCAATCGGTAGTAGCG -3'

Gapdh (Human):

Sense: 5'- GAAGGTGAAGGTCGGAGTC -3'

Antisense: 5'- GAAGATGGTGATGGGATTTC -3'

Gapdh (Mouse):

Sense: 5'- AGGTCGGTGTGAACGGATTTG -3'

Antisense: 5'- GGGGTCGTTGATGGCAACA -3'

B-Actin (Human):

Sense: 5'- AGTCCTGCCCTCATTTCCCT -3'

Antisense: 5'- TGATCTCCTTCTGCATCCTGTC -3'

B-Actin (Mouse):

Sense: 5'- GGCTGTATTCCCCTCCATCG -3'

Antisense: 5'- CCAGTTGGTAACAATGCCATGT -3'

Luciferase:

Sense: 5'- TACGCCGAGTACTTCGAGATGA -3'

Antisense: 5'- CGGGCATGAAGAACTGCAG -3'

EEF1A1 (Human):

Sense: 5'- AGCGTGAACGTGGTATCACCA -3'

Antisense: 5'- TCAAATTCACCAACACCAGCA -3'

FTL (Human):

Sense: 5'- TACGAGCGTCTCCTGAAGATG -3'

Antisense: 5'- AGAACCCAGGGCATGAAGATC -3'

Barcoded DNA oligo RT primer mimic:

PE1 PCR primer template: 5'- CAAGCAGAAGACGGCATACGAGAT[6-bp sample index]CTCTTTCCCTACACGA -3'

- 1. 5'- CAAGCAGAAGACGCATACGAGATACCCTTCTCTTTCCCTACACGA -3'
- 2. 5'- CAAGCAGAAGACGGCATACGAGATAGCACGCTCTTTCCCTACACGA -3'
- 3. 5'- CAAGCAGAAGACGCATACGAGATAAGACACTCTTTCCCTACACGA -3'
- 4. 5'- CAAGCAGAAGACGGCATACGAGATGATTCGCTCTTTCCCTACACGA -3'
- 5. 5'- CAAGCAGAAGACGGCATACGAGATTTCTTACTCTTTCCCTACACGA -3'
- 6. 5'- CAAGCAGAAGACGGCATACGAGATCCCATACTCTTTCCCTACACGA -3'
- 7. 5'- CAAGCAGAAGACGGCATACGAGATCTCCACCTCTTTCCCTACACGA -3'
- 8. 5'- CAAGCAGAAGACGGCATACGAGATCGTTGGCTCTTTCCCTACACGA -3'
- 5'- CAAGCAGAAGACGGCATACGAGATGATCGCCTCTTTCCCTACACGA -3'
- 10. 5'- CAAGCAGAAGACGGCATACGAGATATGTCCCTCTTTCCCTACACGA -3'
- 11. 5'- CAAGCAGAAGACGGCATACGAGATCACGTGCTCTTTCCCTACACGA -3'

- 12. 5'- CAAGCAGAAGACGGCATACGAGATAAACATCTCTTTCCCTACACGA -3'
- 13. 5'- CAAGCAGAAGACGGCATACGAGATCCATCTCTCTTTCCCTACACGA -3'
- 14. 5'- CAAGCAGAAGACGGCATACGAGATTCCAACCTCTTTCCCTACACGA -3'
- 15. 5'- CAAGCAGAAGACGGCATACGAGATGAAGAGCTCTTTCCCTACACGA -3'
- 16. 5'- CAAGCAGAAGACGGCATACGAGATCCACTTCTCTTTCCCTACACGA -3'

PE2 PCR Primer: 5'-

AATGATACGGCGACCACCGAGATCTACACGGTCTCGGCATTCCTGCTGAAC -3'

PE2-N6 RT primer: 5'- TCGGCATTCCTGCTGAACCGCTCTTCCGATCTNNNNNN -3'

Sequencing Primers:

Custom Read 1 Sequencing Primer: 5'-GGCATTCCTGCTGAACCGCTCTTCCGATCT-3'

Custom Read 2 Sequencing Primer: 5'-AGATCGGAAGAGCGTCGTGTAGGGAAAGAG-3'

Custom Indexing Read Primer: 5'-CTCTTTCCCTACACGACGCTCTTCCGATCT-3'

Supplemental Data:

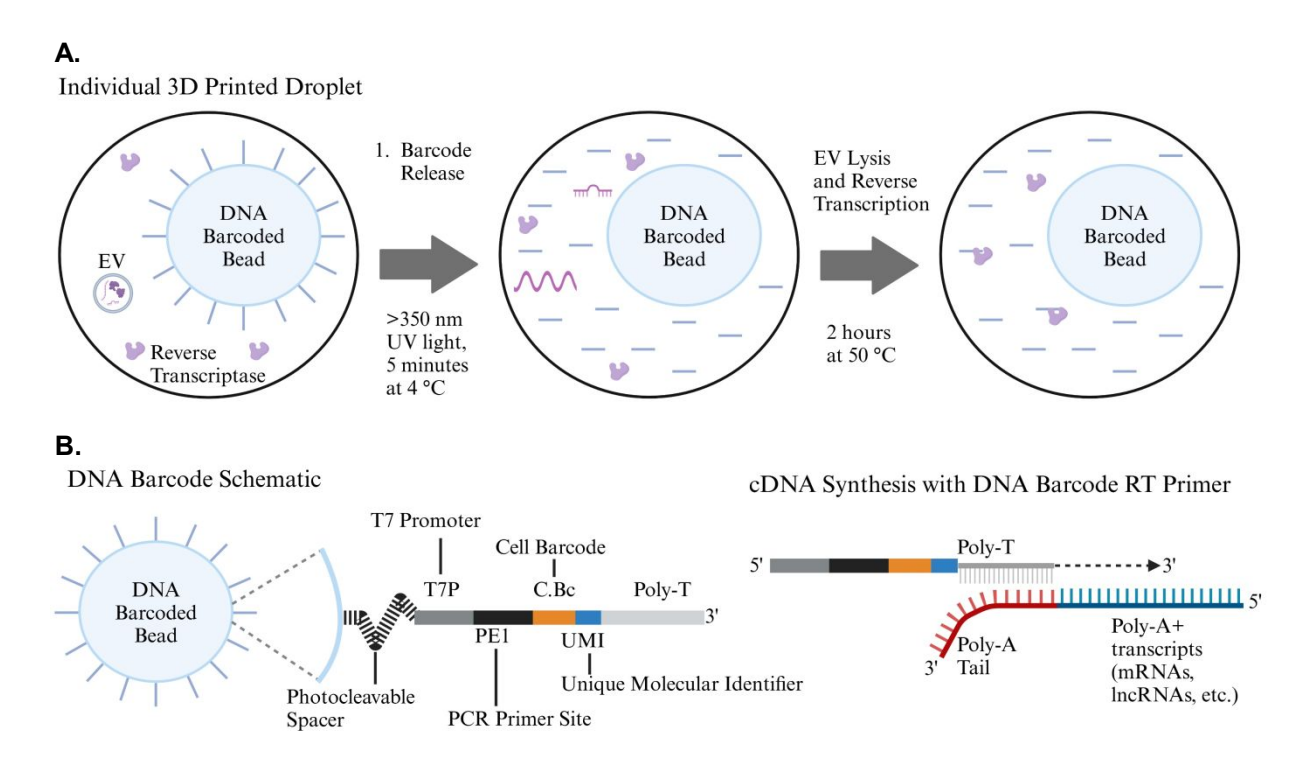


Figure S1. Strategy for single EV sequencing using barcoded beads. (A) Schematic of single EV transcriptome barcoding in droplets. EVs, barcoded hydrogel beads and reverse transcription biochemicals are printed into the microgel where printing is leveraged such that a percentage of the printed droplets will contain one EV and one barcoded hydrogel bead. After EV and hydrogel bead encapsulation, the barcoding cDNA primers are released from the beads using >350-nm UV light, followed by EV lysis at 50° C, poly(A)+ RNA capture and reverse transcription. The cDNA contained within the aqueous phase can be sequenced following standard RNA sequencing library preparations. (B) Schematic of barcoding reverse transcription primers attached to hydrogel beads and the biological components of the DNA barcoded oligo used for library preparation and RNA sequencing. Poly(A)+ RNA is red and blue, and cDNA is the black dashed line.

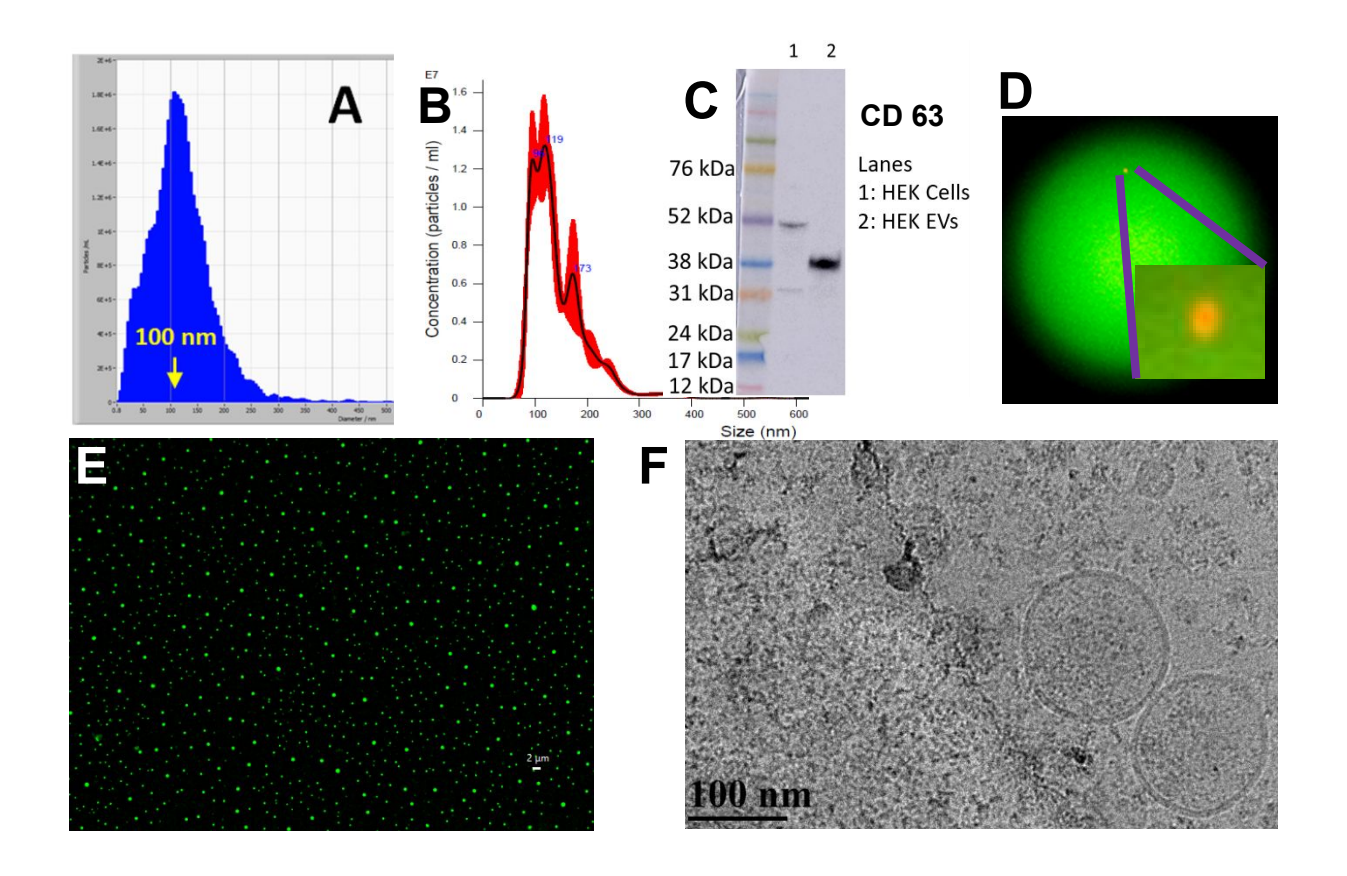
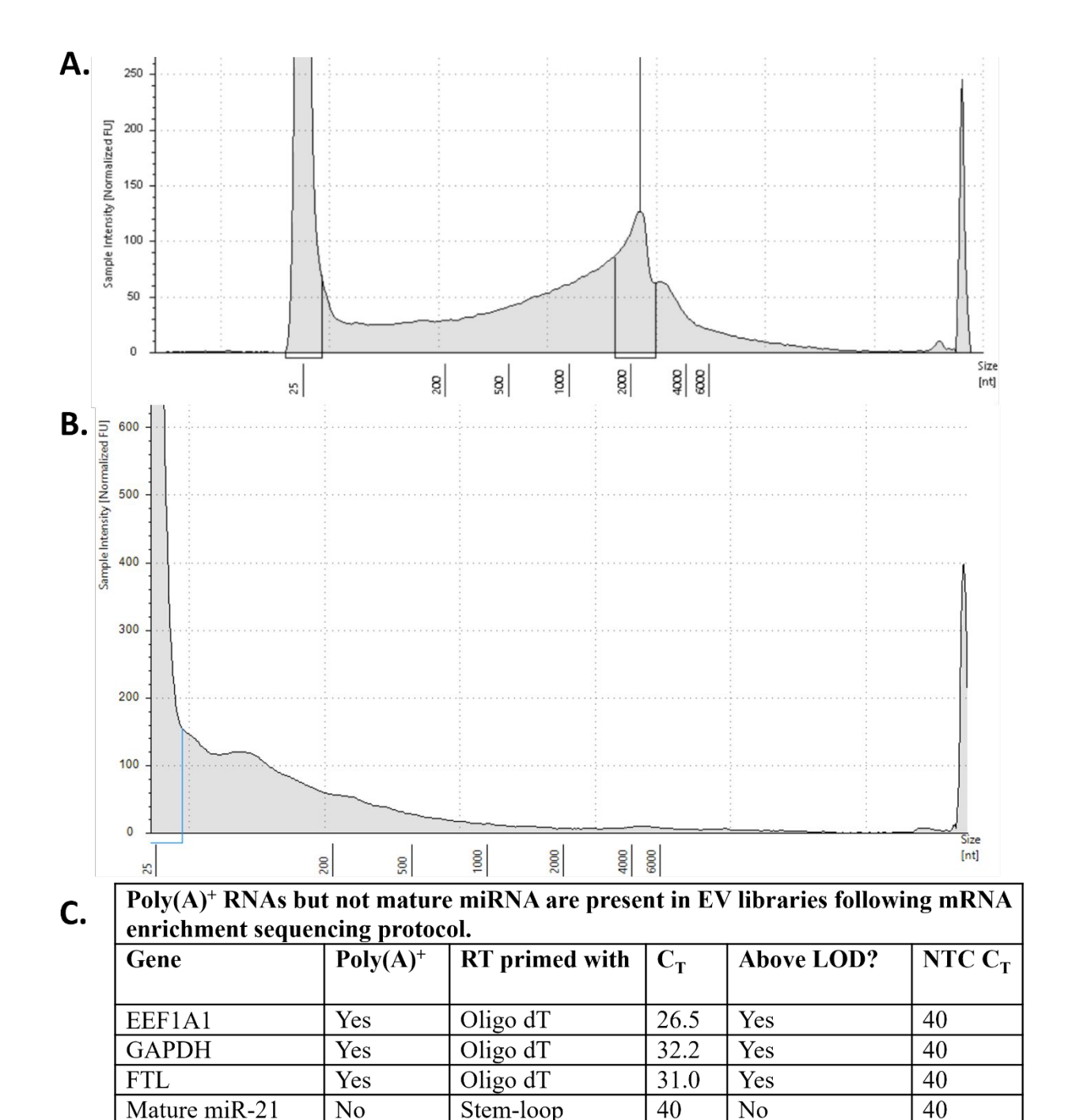


Figure S2. EV characterization. (A and B) ZetaView and NS300 NTA EV particle size distribution and concentration of THP-1 and HEK293T EVs, respectively. NTA shows CD9(+), CD63(+) & CD81(+) THP-1 EVs have an average diameter of 100 nm purified from THP-1 cells using antibody based immunocapture whereas NTA of HEK293T isolated by UC methods have a slightly larger average size of 143.8 nm with a mode of 118.8 nm. (C) HEK293T cells and EVs were probed on a western blot for EV marker CD63. Lanes were loaded with 40 μg of protein. (D) 1 μL of BioTracker 555 Orange Cytoplasmic Membrane dye was used to stain the lipid bilayer of 200 μL of HEK293T EVs to be analyzed by microscopic imaging after 3D printing. Free dye was removed by 3 pelleting steps at 150,000 xg and washing with dPBS. Zeiss LSM 980 confocal microscope was used with 60X water immersion objective to take images. (E) 100 μL HEK293T EVs were stained with 1 μL SYTO RNASelect green fluorescent dye (1 mM) and excess free dye was removed with 3kDa molecular weight cutoff exosome spin column. The image was taken on Keyence All-in-One Fluorescence Microscope BZ-X800 confocal at 100X magnification. Scale bar is 2 μm. (F) Representative cryo-TEM image of HEK293T EVs. Scale bar is 100 nm.



Note: The initial cDNA was synthesized in the printed gel and then combined into a reaction tube for subsequent workup. The assay's LOD is $C_T \le 37$.

40

40

No

No

40

40

Stem-loop

Stem-loop

Mature miR-146a

Mature let-7a

No

No

Figure S3. qRT-PCR of the RNA contents of printed EVs. CD9⁺, CD63⁺ & CD81⁺ EVs or UC isolated EVs with a mean diameter of 100 nm and 130 nm were purified from THP-1 and HEK293T cells, respectively. Approximately 3,500 EVs were printed into the microgel. Oligo dT

labeled beads were used to prime the poly(A)+ RNA, followed by cDNA synthesis in the individual printer droplets of the gel. The aqueous phase containing the cDNA is collected into a reaction tube for subsequent workup including an overnight in vitro transcription (IVT). (A) THP-1 immunopurified EVs Agilent Bioanalyzer results from the IVT reveal the presence of poly(A)+ RNA ranging in size from 200 to 6,000 nt (average 3,537 nt). (B) HEK293T UC purified EVs Agilent Bioanalyzer results from the IVT reveal the presence of poly(A)+ RNA ranging in size from 200 to 6,000 nt. (C) The cDNA synthesized from (A) was assayed by qRT-PCR primed with either oligo dT or stem loop specific primers to the mature miRNA. Results show the presence of the EEF1A1, GAPDH and FTL but the absence of the mature miRNAs.

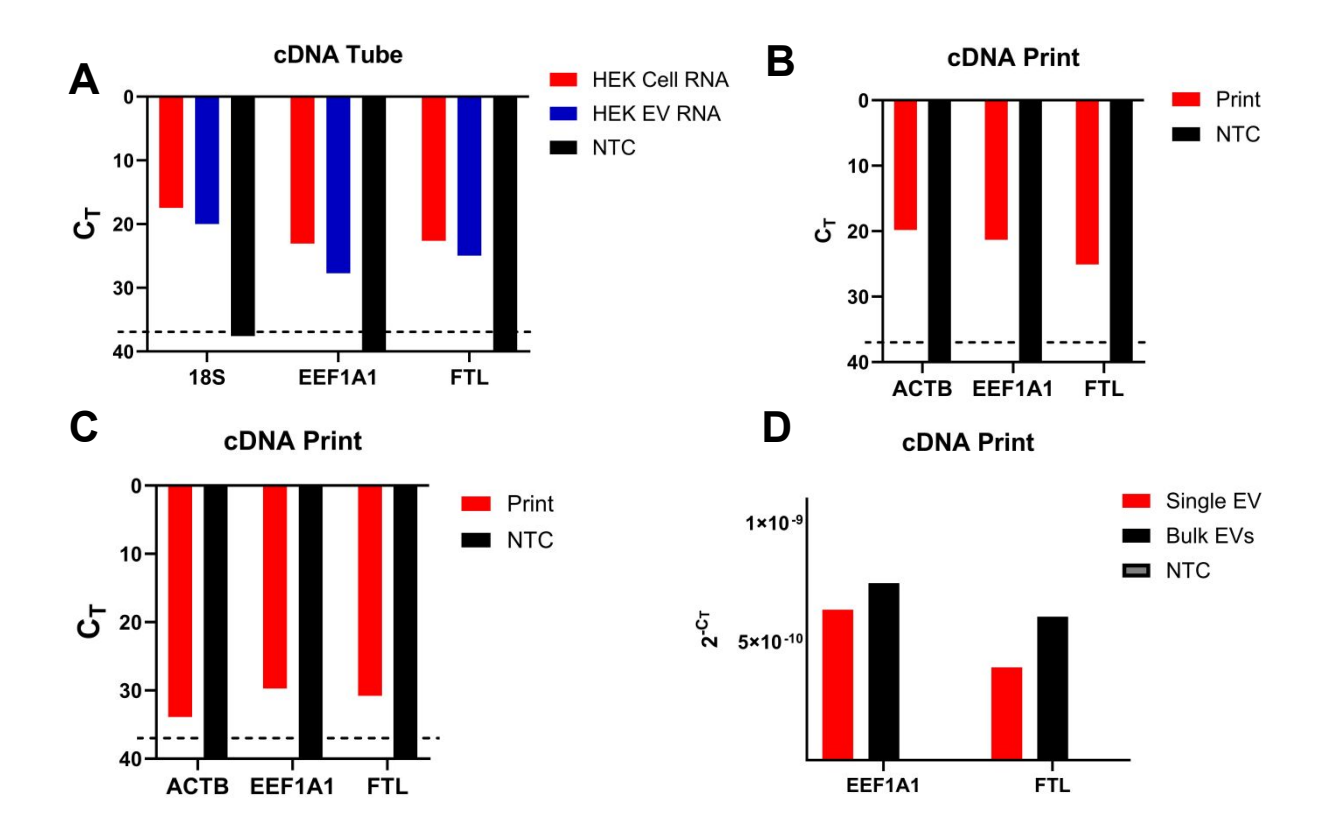


Figure S4. 3D printed and tube biochemical reactions with barcoded DNA hydrogel beads RT primer oligo mimic and barcoded DNA hydrogel beads. (A) A reverse transcription primer mimicking that of barcoded DNA hydrogel bead primer was used to make cDNA with 150 ng of HEK293T cellular and EV RNA in tubes. Expression of 18S, eef1a1, and FTL was detected above the limit of detection. Gene expression analysis of isolated cDNA was subjected to qPCR analysis and data are presented as mean C_T values in triplicate. (B) 3D printed reactions with RT oligo mimic to make cDNA from 150 ng of mouse liver RNA (ACTB) and HEK293T EVs (EEF1A1 and FTL). Gene expression analysis of isolated cDNA was subjected to qPCR analysis and data are presented as mean CT values in triplicate. (C) cDNA from 50 ng of HEK293T EV RNA was made with barcoded DNA hydrogel beads following a 3D printing to generate droplets. Gene expression analysis of isolated cDNA was subjected to qPCR analysis and data are presented as mean C_T values in triplicate. (D) HEK293T EVs were printed in bulk and at single EV conditions. Following cDNA isolation, gene expression analysis of isolated cDNA was subjected to qPCR analysis to detect the presence of eef1a1 and FTL and data are presented as mean 2-CT values in triplicate.

Table S1.

Number of Reads and Genes per EV Identified by Single EV RNA Sequencing

| T | HP-1 CD | 9 ⁺ , CD63 ⁺ , C | D81 ⁺ EVs | HEI | K293T U | JC Purifie | d EVs |
|-------|---------|--|----------------------|-------|---------|------------|-------|
| Reads | EVs | Genes | EVs | Reads | EVs | Genes | EVs |
| 2 | 2381 | 1 | 363 | 2 | 1015 | 1 | 53 |
| 3 | 401 | 2 | 2493 | 3 | 43 | 2 | 995 |
| 4 | 285 | 3 | 413 | 4 | 31 | 3 | 36 |
| 5 | 154 | 4 | 227 | 5 | 4 | 4 | 13 |
| 6 | 113 | 5 | 90 | 6 | 2 | 5 | 2 |
| 7 | 65 | 6 | 46 | 7 | 2 | | |
| 8 | 75 | 7 | 34 | 8 | 0 | | |
| 9 | 50 | 8 | 8 | 9 | 1 | | |
| 10 | 33 | 9 | 10 | 10 | 0 | | |
| 11 | 28 | 10 | 4 | 11 | 1 | | |
| 12 | 21 | 12 | 1 | | | | |
| 13 | 21 | | | | | | |
| 14 | 17 | | | | | | |
| 15 | 13 | | | | | | |
| 16 | 9 | | | | | | |
| 17 | 6 | | | | | | |
| 18 | 6 | | | | | | |
| 20 | 2 | | | | | | |
| 21 | 3 | | | | | | |
| 22 | 1 | | | | | | |
| 23 | 1 | | | | | | |
| 24 | 2 | | | | | | |
| 25 | 1 | | | | | | |
| 33 | 1 | | | | | | |

Expressed Genes in Individual EVs Identified in CD9⁺, CD63⁺, CD81⁺ THP-1 EVs

Table S2.

| | | | Bulk Sequencing Avg. | True Number of Unique |
|---------|--------------|-----|-----------------------|-----------------------------|
| Gene | Unique Reads | EVs | Copies per Printed EV | Reads of Gene in Single EVs |
| ACSS2 | 34 | 3 | .009714 | 2, 16, 16 |
| BOLA3 | 17 | 2 | .004857 | 8, 9 |
| SEC61B | 17 | 2 | .004857 | 6, 11 |
| DZIP1 | 24 | 3 | .006857 | 2, 8, 14 |
| ARHGEF9 | 15 | 2 | .004286 | 6, 9 |
| EPHA4 | 15 | 2 | .004286 | 7, 8 |
| MCM9 | 15 | 2 | .004286 | 6, 9 |
| TFE3 | 15 | 2 | .004286 | 7, 8 |
| SUMF1 | 21 | 3 | .006 | 3, 9, 9 |
| LIN28B | 14 | 2 | .004 | 7, 7 |
| RPS28 | 14 | 2 | .004 | 6, 8 |
| ZFHX2 | 14 | 2 | .004 | 6, 8 |